Journal of Experimental Botany, Vol. 75, No. 10 pp. 2900–2916, 2024
https://doi.org/10.1093/jxb/erae044 Advance Access Publication 15 February 2024

RESEARCH PAPER

HOMEOBOX2, the paralog of SIX-ROWED SPIKE1/ HOMEOBOX1, is dispensable for barley spikelet development

Venkatasubbu Thirulogachandar[1,2,†,*], Geetha Govind[1,‡], Götz Hensel[1,§], Sandip M. Kale[1,¶], Markus Kuhlmann[1,2], Lennart Eschen-Lippold[3,††], Twan Rutten[1], Ravi Koppolu[1], Jeyaraman Rajaraman[1], Sudhakar Reddy Palakolanu[1,‡‡], Christiane Seiler[1,§§], Shun Sakuma[4,¶¶], Murukarthick Jayakodi[1], Justin Lee[3], Jochen Kumlehn[1], Takao Komatsuda[4,†††], Thorsten Schnurbusch[1,5,*], and Nese Sreenivasulu[1,2,‡‡‡,*]

[1] Leibniz Institute of Plant Genetics and Crop Plant Research (IPK), Corrensstr. 3, OT Gatersleben, D-06466 Stadt Seeland, Germany
[2] Research Group Abiotic Stress Genomics, Interdisciplinary Center for Crop Plant Research (IZN), Hoher Weg 8, 06120 Halle (Saale), Germany
[3] Leibniz Institute of Plant Biochemistry (IPB), Weinberg 3, D-06120 Halle, Germany
[4] National Institute of Agrobiological Sciences (NIAS), Plant Genome Research Unit, Tsukuba 3058602, Japan
[5] Institute of Agricultural and Nutritional Sciences, Faculty of Natural Sciences III, Martin Luther University Halle-Wittenberg, 06120 Halle, Germany
[†] Present address: Institute of Plant Genetics, Heinrich Heine University, 40225 Düsseldorf, Germany.
[‡] Present address: Department of Crop Physiology, College of Agriculture, Hassan, 573225, Karnataka, India.
[§] Present address: Institute of Plant Biochemistry, Heinrich Heine University, 40225 Düsseldorf, Germany.
[¶] Present address: Crop Genetics and Biotechnology Section, Department of Agroecology, Forsøgsvej 1, 4200 Slagelse, Denmark.
[††] Present address: Department of Crop Physiology, Institute of Agricultural and Nutritional Sciences, Martin Luther University, 06120 Halle-Wittenberg, Germany.
[‡‡] Present address: Cell, Molecular Biology, and Trait Engineering Cluster, International Crops Research Institute for the Semi-Arid Tropics (ICRISAT), Hyderabad, 502 324, Telangana, India.
[§§] Present address: Institute for Resistance Research and Stress Tolerance, Julius Kuehn Institute (JKI), 06484 Quedlinburg, Germany.
[¶¶] Present address: Faculty of Agriculture, Tottori University, Tottori 680-8550, Japan.
[†††] Present address: Crop Research Institute, Shandong Academy of Agricultural Sciences (SAAS), Jinan, Shandong 250100, China.
[‡‡‡] Present address: International Rice Research Institute (IRRI), Grain Quality and Nutrition Center, DAPO Box 7777, Metro Manila, Philippines.

* Correspondence: n.sreenivasulu@irri.org, schnurbusch@ipk-gatersleben.de, or thirulogachandar.venkatasubbu@hhu.de

Received 4 September 2023; Editorial decision 31 January 2024; Accepted 14 February 2024

Editor: Mary Byrne, University of Sydney, Australia

Abstract

The HD-ZIP class I transcription factor Homeobox 1 (HvHOX1), also known as Vulgare Row-type Spike 1 (VRS1) or Six-rowed Spike 1, regulates lateral spikelet fertility in barley (*Hordeum vulgare* L.). It was shown that *HvHOX1* has a high expression only in lateral spikelets, while its paralog *HvHOX2* was found to be expressed in different plant organs. Yet, the mechanistic functions of HvHOX1 and HvHOX2 during spikelet development are still fragmentary. Here, we show that compared with *HvHOX1*, *HvHOX2* is more highly conserved across different barley genotypes and *Hordeum* species, hinting at a possibly vital but still unclarified biological role. Using bimolecular fluorescence complementation,

DNA-binding, and transactivation assays, we validate that HvHOX1 and HvHOX2 are bona fide transcriptional activators that may potentially heterodimerize. Accordingly, both genes exhibit similar spatiotemporal expression patterns during spike development and growth, albeit their mRNA levels differ quantitatively. We show that HvHOX1 delays the lateral spikelet meristem differentiation and affects fertility by aborting the reproductive organs. Interestingly, the ancestral relationship of the two genes inferred from their co-expressed gene networks suggested that HvHOX1 and HvHOX2 might play a similar role during barley spikelet development. However, CRISPR-derived mutants of *HvHOX1* and *HvHOX2* demonstrated the suppressive role of HvHOX1 on lateral spikelets, while the loss of HvHOX2 does not influence spikelet development. Collectively, our study shows that through the suppression of reproductive organs, lateral spikelet fertility is regulated by HvHOX1, whereas HvHOX2 is dispensable for spikelet development in barley.

Keywords: Anther and pistil development, barley (*Hordeum vulgare*), CRISPR, gene duplication, HD-ZIP class I transcription factors, inflorescence architecture, nucleotide diversity, spikelet fertility.

Introduction

Cereals such as maize (*Zea mays* L.), rice (*Oryza sativa* L.), wheat (*Triticum* spp.), and barley (*Hordeum vulgare* L.) are major grass species that feed most of the world's population. Understanding the genetic regulation of inflorescence (flower-bearing structure) architecture in these cereal crops may shed light on the basic developmental patterning of floral meristems and reveal potential pathways to improve their yield. Barley, along with other major cereal crops (wheat, rye, and triticale) belonging to the Triticeae tribe, possesses a spike-type inflorescence (Ullrich, 2011; Koppolu and Schnurbusch, 2019). In general, a barley spike forms three spikelets on its rachis (inflorescence axis) nodes—one central and two lateral spikelets in an alternating, opposite arrangement (distichous) (Bonnett, 1935; Koppolu and Schnurbusch, 2019; Zwirek *et al.*, 2019). The spikelet, a small/condensed spike, is considered the basic unit of the grass inflorescence (Clifford *et al.*, 1987; Kellogg *et al.*, 2013). A barley spikelet forms a single floret subtended by a pair of glumes. Typically, a barley floret consists of one lemma, one palea, two lodicules, three stamens, and a monocarpellary pistil (i.e. a single carpel) (Waddington *et al.*, 1983; Forster *et al.*, 2007). Based on the fertility of the lateral spikelets/florets, barley is classified into two- and six-rowed spike types. In two-rowed types, the lateral spikelets are smaller (compared with the central spikelets), awnless (extension of the lemma is absent), and sterile, while the central spikelets are bigger, awned, and fertile. Both the lateral and central spikelets are awned and fertile in six-rowed types.

The major gene responsible for the lateral spikelet sterility was found to be a homeodomain leucine zipper class I (HD-ZIP I) transcription factor (TF), known as *Homeobox 1* (*HvHOX1*), *Vulgare Row-type Spike1* (*VRS1*) or *Six-rowed Spike 1* (Komatsuda *et al.*, 2007; Thirulogachandar *et al.*, 2017), herein referred to as *HvHOX1*. Transcripts and proteins of *HvHOX1* had previously been found in barley spikes, predominantly in the lateral florets and most strongly in the lateral spikelet carpels, corroborating the role of HvHOX1 as a suppressor of lateral floret development and fertility (Komatsuda *et al.*, 2007; Sakuma *et al.*, 2010, 2013). A similar function has also been identified for its orthologous wheat gene during apical floret abortion (Sakuma *et al.*, 2019). *HvHOX1* was shown to be also expressed in leaves, wherein, in analogy to its effects on lateral spikelets, it decreased the size of leaf primordia, resulting in narrower leaves in two-rowed barleys (Thirulogachandar *et al.*, 2017). Further supporting its suppressive function, one specific allele of *HvHOX1* in *deficiens* barley is responsible for extremely reduced lateral spikelet/floret sizes (Sakuma *et al.*, 2017). Interestingly, *HvHOX2*, the paralog of *HvHOX1*, was also identified in barley and is expressed in various organs, including leaves, coleoptile, root, and spike. Tissue-wise, it is mainly found in vascular regions, particularly those at the base of lateral spikelets (pedicel) and rachis, and is thus projected to play a role in the promotion of development (Sakuma *et al.*, 2010, 2011, 2013). In addition to *HvHOX1*, four other genes, *VRS2*, *VRS3*, *VRS4*, and *VRS5* or *INT-C* (*intermedium-spike c*), were reported to be involved in the suppression of lateral spikelet fertility (Ramsay *et al.*, 2011; Koppolu *et al.*, 2013; Bull *et al.*, 2017; van Esse *et al.*, 2017; Youssef *et al.*, 2017). Notably, VRS4, the ortholog of maize RAMOSA2 (RA2), appeared to be an upstream regulator of *HvHOX1* but not of *HvHOX2* (Koppolu *et al.*, 2013; Sakuma *et al.*, 2013). Later, VRS3 was also identified as an upstream regulator of *HvHOX1* and, in certain stages, also of *HvHOX2* (Bull *et al.*, 2017; van Esse *et al.*, 2017).

Despite the detailed studies on HvHOX1's role in suppressing lateral spikelets, the mechanistic role of how HvHOX2 operates during barley spikelet development is still unclear (Sakuma *et al.*, 2010, 2013). This study clarifies that HvHOX1 and HvHOX2 proteins are functional HD-ZIP class I TFs in spite of a significant difference in their nucleotide diversity. Our transcript expression studies suggest that both have similar spatiotemporal expression patterns; however, mostly, transcript levels in central and lateral spikelets during spikelet development and growth are significantly different. Their co-expression gene networks validated their ancestral relationship

and suggested that they might play a similar role during barley spikelet development. We reveal that HvHOX1 impacts lateral spikelet fertility by aborting the reproductive organs. Our *Hvhox1*, *Hvhox2*, and double CRISPR mutants indicate that HvHOX2 is not a negative regulator of spikelet development, whereas HvHOX1 affects barley lateral spikelet fertility.

Materials and methods

Plant materials and their growth conditions

Barley cultivars Bonus, Bowman, and Golden Promise were used in this study as two-rowed representatives, and induced mutant *hex-v.3* (progenitor cv. Bonus), cultivar Morex, and Bowman backcross-derived line BW-NIL(*vrs1.a*)/BW 898 (Druka *et al.*, 2011) were used as six-rowed representatives. Wild species of *Hordeum* were obtained from Dr. Roland von Bothmer, Swedish University of Agricultural Sciences, Alnarp, Sweden (Supplementary Table S1). Arabidopsis Col-0 plants were used for protoplast isolations and grown on a 1:3 vermiculite: soil mixture in a phytochamber (8 h light–16 h dark at 20 °C and 18 °C, respectively; light intensity 140 µmol m^{-2} s^{-1}; 60% humidity). Barley plants were grown on the substrate containing four parts of autoclaved compost, two parts of 'Rotes Substrat' (Klasmann-Deilmann GmbH, Germany), 1.6 parts of sand, and 0.8 parts of peat. Grains were planted in either 54- or 96-well plastic trays and germinated in a climate chamber or temperature-controlled greenhouse for 4 weeks at 11 °C day and 7 °C night with 10 h light (light intensity 270 µmol m^{-2} s^{-1} (climate chamber); 300–500 µmol m^{-2} s^{-1} (greenhouse)). After 4 weeks of growth, seedlings were transferred to pots (diameter 16, 11, or 14 cm) and allowed to mature in the greenhouse. Further growth conditions were divided into four phases: first phase at 14 °C day and 9 °C night with 12 h light for 4 weeks; second phase at 16 °C day and 9 °C night with 14 h light for 2 weeks; third phase at 20 °C day and 12 °C night with 16 h light for 2 weeks; and fourth phase at 20 °C day and 14 °C night with 16 h light until harvest. Plants were fertilized with 'Plantacote plus' (Aglukon GmbH, Germany) (15 g/pot) during the vegetative phase and with liquid fertilizer 'Hakaphos Rot' (Aglukon GmbH, Germany) (once a week, 2–4%) from the start of spike development.

Nucleotide diversity calculation

The whole-genome sequencing (WGS) data and single nucleotide polymorphism (SNP) matrix for 200 diverse barley genotypes were downloaded from Jayakodi *et al.*, 2020. The sequencing reads were aligned to the reference cv. Morex, as described (Jayakodi *et al.*, 2020). The effectively covered areas of the barley genome were identified by the regions covered by at least two reads in ≥80% of the WGS accessions. The nucleotide diversity (π) was calculated on a 10 kb window with a step size of 2 kb with a custom script. Only the windows with ≥2 kb effectively covered region were considered.

Resequencing of HvHOX1 *and* HvHOX2

Genomic DNA was extracted as described (Komatsuda *et al.*, 1998). PCR primers were designed using Oligo5 software (W. Rychlick, National Bioscience, Plymouth, MN, USA) and synthesized commercially (BEX, Tokyo, Japan). Primer information can be found in Supplementary Table S2. PCR amplification was carried out in 50 µl reactions containing 1.25 U ExTaq polymerase (Takara, Tokyo, Japan), 1× ExTaq polymerase buffer, 0.3 µM of each primer, 200 µM dNTPs, 2 mM $MgCl_2$, 2.5% (v/v) dimethyl sulfoxide, and 100 ng genomic DNA. Each PCR was cycled through a denaturation step (94 °C/5 min), followed by 30 cycles of 94 °C/30 s, 55 °C/30 s, 72 °C/60 s with a final incubation of 72 °C/7 min. PCR products were purified using the QIA-quick PCR purification Kit (Qiagen, Hilden, Germany) and subjected to cycle sequencing using a Big Dye Terminator Kit (Thermo Fisher Scientific, Waltham, MA, USA). Sequencing reactions were purified by Agencourt CleanSEQ (Beckman Coulter, Brea, CA, USA) and analysed with an ABI prism 3130 genetic analyser (Thermo Fisher Scientific). Levels of nucleotide diversity per site were estimated by the parameter π (Nei, 1987) using DnaSP v5.00.03 software (Rozas *et al.*, 2003).

TILLING and resequencing of HvHOX2

To identify the *HvHOX2* mutants, an ethyl methanesulfonate-treated targeting induced local lesions in genomes (TILLING) population derived from cv. Barke was screened (Gottwald *et al.*, 2009). For mutation screening, the primers spanning the open reading frame (ORF) of *HvHOX2* were used. The TILLING primer sequences can be found in Supplementary Table S2. Procedural details of TILLING can be found in Gawroński *et al.* (2014). For resequencing of *HvHOX2*, three primer pairs were designed to amplify promoter, coding sequence, and 3′-untranslated region (UTR). The amplicons generated were Sanger sequenced and assembled using Seqman 8.0.2 (DNASTAR, Inc.). SNP calling was done by visual inspection of sequence chromatograms. The details of *HvHOX2* resequencing primers can be found in Supplementary Table S2.

In silico *identification of genes*

The CDSs of the *HvHOX1* (*VRS1*) gene (Version: AB259782.1, GI: 119943316) was taken from the NCBI database and used to design primers for amplifying the *HvHOX1* CDS. The same approach was followed for the *HvHOX2* gene (Version: AB490233.1, GI: 266265607).

Preparation of constructs

The coding sequences (CDS) of *HvHOX1* and *HvHOX2* were amplified from their respective pCR4.0-TOPO vectors (constructed for transformation studies) and cloned into a Gateway-compatible pCR8/GW/TOPO vector (Thermo Fisher Scientific, Schwerte, Germany). In the following, both the CDSs were cloned into pHBTL-35s-GBD-GW vectors (Gateway compatible, GAL4 DNA binding domain fusions) (Ehlert *et al.*, 2006) by recombination-mediated Gateway cloning according to the manufacturer's instructions and the resultant vectors (minimum three) were validated for the integrity of the cloned fragments by sequencing.

Bimolecular fluorescence complementation assay

A protein–protein interaction study was done using a bimolecular fluorescence complementation (BiFC) assay in Arabidopsis mesophyll protoplasts. The pCR8/GW/TOPO cloned *HvHOX1* CDS and *HvHOX2* CDS (explained above) were recombined into both pE-SPYNE (N-terminal half of yellow fluorescent protein (YFP)) and pE-SPYCE (C-terminal half of YFP) vectors using recombination-mediated Gateway cloning according to the protocols of the manufacturer (Thermo Fisher Scientific). The use of these vectors resulted in the fusion of YFP fragments to the N-terminal part of HvHOX1 and HvHOX2 proteins. The pE-SPYNE vector expressing a split YFP-domain alone was used as a negative control. A plasmid carrying *Cyan Fluorescence Protein* (*CFP*) driven by p35S promoter was co-transformed as a reference for nuclear/cytoplasmic localization. The protoplasts were isolated and transformed following polyethylene glycol-mediated transformation (Yoo *et al.*, 2007) with 10 µg each of pE-SPYNE harboring *HvHOX1* or *HvHOX2*, pE-SPYCE harboring *HvHOX1* or *HvHOX2* and *CFP* (0.3 ml total transformation volume), respectively, and incubated for 16 h in the dark. The interaction and subcellular localization were visualized by fluorescence

microscopy using the LSM 710 Laser Scanning System (Carl Zeiss). The excitation wavelengths and emission filters were 514 nm/bandpass 505–530 nm for YFP, 458 nm/bandpass 465–530 nm for CFP, and 488 nm/bandpass 650–710 nm for chloroplast auto-fluorescence.

Western blot analysis

Proteins were extracted from protoplasts used for protein interaction studies by boiling in a standard SDS-loading buffer. Proteins were separated by 12.5% SDS-PAGE and transferred to a nitrocellulose membrane (Macherey-Nagel GmbH) by blotting. Immune detection was performed using primary anti-c-myc (c-myc-nYFP-fusion proteins) (Sigma-Aldrich) and anti-HA.11 (HA-cYFP-fusion proteins) (Eurogentec) antibodies, followed by a horseradish peroxidase-coupled secondary anti-mouse antibody (Sigma-Aldrich).

Electrophoretic mobility shift assay

The CDSs of *HvHOX1* and *HvHOX2* were amplified from their respective vectors cloned for transgenic analysis (explained above) and fused to the T7-promotor sequence according to the manufacturer's protocol (PURExpress, New England Biolabs). After verifying the integrity of cloned fragments by sequencing, the proteins HvHOX1 and HvHOX2 were synthesized by the novel cell-free transcription/translation system PURExpress according to the manufacturer's protocol. An electrophoretic mobility shift assay (EMSA) was performed as described previously (Kuhlmann *et al.*, 2003). The binding sequences (BS) (putative *cis*-element) of HD-Zip I proteins shown earlier (Sessa *et al.*, 1993) were used as arbitrary primers for this mobility assay. All primers and binding sequences are given in Supplementary Table S2.

Transactivation assay

Isolation and transformation of Arabidopsis mesophyll protoplasts were performed according to the method described previously (Yoo *et al.*, 2007). Protoplasts were transformed with *HvHOX1*/*HvHOX2*-GAL4 binding domain fusion constructs, a pGAL4-4×UAS::GUS reporter construct (Ehlert *et al.*, 2006) and a p35S-LUC plasmid for normalization. For one transformation, a total of 50 μg plasmid DNA per 500 μl protoplasts was used (constructs were transformed in equal amounts). After transformation (n=3), protoplasts were aliquoted in five samples each. After 16 h, luciferase (LUC) activity was measured in living protoplasts as previously described (Ranf *et al.*, 2011). Protoplasts were then lysed in GUS extraction buffer (50 mM $NaPO_4$ pH 7.0, 1 mM EDTA, 0.1% Triton X-100, and 10 mM β-mercaptoethanol) by vortexing. β-Glucuronidase (GUS) activity was measured upon incubation with 4-methylumbelliferyl glucuronide (15 min at 37 °C), based on the fluorometric detection of the reaction product 4-methylumbelliferone (at 360 nm/460 nm). Values are expressed as GUS/LUC ratios.

Histology of anther, carpel, and spike development

Spikes were dissected under a Zeiss Stemi SV 11 stereoscope (Carl Zeiss Microscopy GmbH, Jena, Germany) from two-rowed barley cv. Bowman and six-rowed barley (*vrs1.a*) mutant BW-898. Dissected samples were fixed in a fixative containing 4% formaldehyde, and 1% glutaraldehyde in 50 mM phosphate buffer for 5–9 d at 4 °C. Fixed samples were washed once in phosphate buffer and twice in distilled water at room temperature for 15 min. Then, washed samples were incubated in 1% osmium tetraoxide (OsO4) for 1 h at room temperature, followed by two washes with distilled water. Samples were dried by ethanol gradient (30%, 50%, 70%, 90%, and two times in 100%) for 15 min at room temperature for each ethanol solution. Dried samples were incubated in 100% propylenoxid at room temperature. Finally, samples were polymerized in a Spurr resin gradient (25% overnight, 50% 4 h, 75% 4 h, and 100% overnight) and then kept in an oven at 700 °C for 24 h. Polymerized samples were sectioned at 10 μm thickness using a Reichert-Jung Ultracut microtome (Leica) and fixed on glass slides. Finally, samples were imaged with a Zeiss Axio Imager light microscope (Carl Zeiss Microscopy GmbH, Jena, Germany) at ×20 magnification.

Light microscopy

Two different types of light microscopes were used for taking images or (micro) phenotyping of spike meristem development. All histological images of the anther and pistil were taken with a Zeiss Axio Imager light microscope, and the images were processed with Axiovision SE64 release 4.8 software (Carl Zeiss Microscopy). A Zeiss Stemi 2000-C stereomicroscope with Axiovision release 4.8.2 software was used to identify the developmental stage of the spike meristem.

Scanning electron microscopy

Chemically fixed samples like the spike meristem and spikelet organs were washed once in 50 mM phosphate buffer and twice in distilled water at room temperature for 15 min. Then, washed samples were dehydrated in an ethanol gradient (30%, 50%, 70%, 90%, and two times in 100%), each step lasting 15 min. The samples were dried at their critical point in a BAL-TEC critical point dryer, CPD 030 (BAL-TEC GmbH, Germany). Finally, the dried samples were placed on a scanning electron microscopy (SEM) specimen holder and gold-sputtered with an Edwards Sputter Coater S150 B (Edwards GmbH, Germany). The gold deposition was done in the presence of argon gas with 0.3 mbar pressure, and samples were examined with a scanning electron microscope (model S4100; Hitachi, Tokyo, Japan) at an accelerating voltage of 10 kV. The images were scanned with Digital Image Scanning System (DISS 5) v5.10 software and processed by Digital Image Processing System (DIPS) v2.9 software (Point Electronic GmbH, Germany).

Fluorescence microscopy

Fluorescence was analysed with either an LSM 780 or an LSM 510 META confocal laser scanning microscope (Carl Zeiss). In the LSM 710, green fluorescent protein (GFP) was visualized with the excitation from a 488 nm wavelength argon laser in combination with a dichroic beam splitter, a 488 nm main beam splitter (MBS), and the emission filter was 490–660 nm. The chlorophyll was visualized with excitation from a 633 nm wavelength helium–neon laser in combination with 488/561/633 nm MBS, and the emission filter was 644–680 nm. Cell wall autofluorescence was captured with the excitation from a 405 nm wavelength diode laser and 405 nm MBS and 417–507 nm emission filter.

With the LSM 510 META microscope, GFP was visualized with excitation by a 488 nm argon 2 laser in combination with a 505–530 nm bandpass filter. The chlorophyll in the samples was detected with the excitation by a 633 nm helium–neon 2 (HeNe2) laser in combination with a 650 nm long-pass filter and cell wall autofluorescence with the excitation of a 364 nm Enterprise laser line in combination with 385 nm long-pass filter. In all samples, the authenticity of the GFP signal was analysed by photospectrometric unmixing using a lambda detector.

RNA isolation and cDNA synthesis

Whole spike, central, and lateral spikelets were collected from respective stages using a Zeiss Stemi 2000-C stereomicroscope. The central and lateral spikelets were carefully dissected from the middle of the spike (synchronously developed spikelets) using forceps under the microscope. RNA from the collected materials was isolated using an absolute Qiagen Plant RNA preparation kit, according to the manufacturer's protocol,

which included the on-column DNaseI treatment. The RNA quality was analysed using an Agilent Bioanalyzer 2100 (Agilent Technologies, Walbronn, Germany). RNA was isolated from three independent biological replicates, and each replicate was a pool of a minimum of five spike meristems. Total RNA, 0.5 μg or 1 μg, was used for first-strand cDNA synthesis primed by oligo-dT primers using Superscript III (Thermo Fisher Scientific) or RevertAid cDNA kit (Thermo Fisher Scientific) following the manufacturer's protocols.

Microarray probe preparation and data analysis

The microarray probe preparation, hybridization, and data analysis were done as previously reported (Thirulogachandar *et al.*, 2017). Total RNA samples isolated from barley spike meristem, shoot apical meristem, and spikelets were labeled using the Low Input Quick Amp Labeling kit (Agilent Technologies) according to the One-Color Microarray-Based Gene Expression Analysis protocol supplied by the manufacturer. Hybridization and washing of chips were also done by the manufacturer's protocol. Finally, the chips were scanned at a high resolution of 2 μm using an Agilent DNA Microarray Scanner G2565CA. The resulting TIFF images were used to run batch extractions with the selection-appropriate grid using Agilent Feature Extraction Software v11.0. The evaluation metrics of each sample were assessed with the manufacturer's standards using the quality control (QC) report, and only samples meeting those standards were taken for further analysis. The QC-verified raw data generated from our custom synthesized 60k barley microarray was analysed by GeneSpring v13.0 (Agilent Technologies). By using Agilent Single Color Workflow along with Data Import Wizard type, the raw data (entities) was thresholded to raw signal intensities of 1.0, quantile normalized, and baseline transformed to the median of all samples. After this, the entities were filtered by the following four steps: (i) in a Filter Probesets by Expression step, the low-expressed entities were removed by setting the low expression value to 25; (ii) in a Filter Probesets by Flags step, the entities were filtered based on the flag values of 'detected', 'non-detected', or 'both'; (iii) in a Filter Probesets on Datafiles step, the Control ProbeSets, which are included in the chip, were removed; and finally (iv) in a Filter ProbeSets by Error step, the entities were filtered by coefficient of variation (CV)<50%, which completed the pre-processing of sample data. The statistical analysis was done with an error (CV<50%)-filtered entity set, using a moderated *t*-test along with the Bonferroni–Holm or Benjamini–Hochberg multiple testing corrections and *P*-value cut-off of ≤0.05. Entities having a fold change of ≥2.0 were taken for data interpretation.

Data preparation and co-expression network construction

The processed normalized data for each genotype were used for co-expression network construction. Initially, hierarchical clustering analysis was carried out for each genotype to remove the replicates that failed to cluster together. Then, the CV within replicates for different time points for each probe was calculated. The probes having CV≤ 20% among 50% of tissues were selected for the construction of a gene co-expression network.

The Weighted Gene Co-Expression Network Analysis (WGCNA) package (Langfelder and Horvath, 2008) was run on R (version 3.3.2) for network construction and module identification using default parameters, except: networkType='signed', softPower=14, minModuleSize=30, deepSplit=4, and MEDissThres=0.15. The other parameters were set to default. In brief, a weighted correlation network was created by calculating the correlation coefficients with the power β=14, which was selected based on the criterion of approximate scale-free topology. The network was then transformed into a network of topological overlap (TO), which considers not only the correlation of two genes with each other but also the extent of their shared correlations across the weighted network (Langfelder and Horvath, 2008). Hierarchical clustering was carried out using the TO matrix to group highly co-expressed genes. The dynamic tree-cut algorithm was then used for tree-cutting and module identification (Langfelder and Horvath, 2008). The most representative gene expression pattern of the module was determined using the singular value decomposition method (Langfelder and Horvath, 2008). The WGCNA exportNetworkToCytoscape function was used to export the probe connections and their scores for each module. The network visualization was done using Cytoscape (V3.6.1.).

Gene ontology enrichment analysis

The gene ontology (GO) enrichment analysis of differentially expressed genes and gene modules was done using the agriGO platform (v2) (Tian *et al.*, 2017). The selected genes' Arabidopsis IDs were queried against the Arabidopsis genome locus (TAIR9) reference set with Fisher's statistical test, Hochberg (false discovery rate) multi-test adjustment method, and a significance level of 0.05. The Plant GO slim 'GO type' was selected with a minimum number of entries. For final interpretation, the GO enrichment of biological processes was used.

Genomic DNA extraction

Genomic DNA was extracted from leaves, which were collected in 2 ml Eppendorf tubes containing two small metal balls and then frozen in liquid nitrogen. Frozen samples were ground with TissueLyser II (Qiagen) to a fine powder. The samples were lysed by adding 800 μl of extraction buffer (1% *N*-lauryl-sarcosin, 100 mM Tris–HCl pH 8.0, 10 mM EDTA, 100 mM NaCl) and mixed vigorously in a standard lab vortexer for 2 min. Then, 800 μl of phenol/chloroform/iso-amyl alcohol (25:24:1) was added and the mixture vortexed for 2 min. Immediately, tubes were centrifuged at 18 312 *g* for 3 min at 25 °C or room temperature; 700 μl of supernatant was carefully aspirated from the centrifuge tubes and dispensed into new 1.5 ml Eppendorf tubes. Nucleic acids were precipitated by adding 70 μl of 3 M sodium acetate (pH 5.2) and 700 μl of isopropanol, mixed briefly, and then precipitation was enhanced by centrifuging the tubes at 17949 *g* for 10 min at 4 °C. Supernatants were carefully aspirated, and the remaining white pellets were washed with 500 μl of 70% ethanol and precipitated by centrifugation at 17949 *g* for 5 min at 4 °C. Again, the supernatants were carefully aspirated, and the pellets were dried at 37 °C for 1 h. The pellets were finally dissolved in 50–100 μl of Tris–HCl (pH 8.0) containing RNase (0.5 μg μl^{-1}) and incubated at 37 °C for 1 h.

Cloning of HvHOX1 *and* HvHOX2 *genes and their respective promoters*

The CDSs of *HvHOX1* and *HvHOX2* were PCR amplified from the inflorescence meristem's cDNA of cultivar Bonus (two-rowed barley) using CDS-specific forward and reverse primers. The same sequences were used as queries in the 'IPK Barley BLAST server', and their upstream promoter sequences were identified. Then, the promoter sequences (along with the 5′-UTR) of both genes were amplified from the leaf genomic DNA of the same cultivar using the promoter-specific primers. The amplified nucleotide fragments (CDSs and promoters) were cloned into pCR4-TOPO TA (Thermo Fisher Scientific). All the plasmids containing CDSs and promoter sequences were sequenced (at least three PCR-positive plasmids for each fragment) to verify the integrity of CDS and promoter sequences. A plasmid having the fragment (CDS or promoter) without any sequencing error was used for further cloning.

Construction of promoter–gene cassettes and plant transformation

HvHOX2 promoter (1929 bp) was amplified by HvHOX2 Promoter Ext-F and HvHOX2 Promoter Int-R primers and subcloned into the pCR4.0-TOPO vector. Then, using HvHOX2 Promoter StuI-F and

HvHOX2 Promoter PstI-R primers, the *HvHOX2* promoter was 'directionally' cloned into the pNOS-AB-M (DNA cloning service, Hamburg, Germany) vector's multiple cloning sites via *Stu*I and *Pst*I sites. The resultant plasmid was renamed *pNOS-HvHOX2* promoter. Similarly, the *HvHOX1* (991 bp) promoter was amplified using HvHOX1 Promoter Ext-F and HvHOX1 Promoter Int-R primers, subcloned into the pCR4.0-TOPO vector, and using HvHOX1 Promoter BamHI-F and HvHOX1 Promoter PstI-R primers, it was cloned into the pNOS-AB-M vector. Similarly, *eGFP* CDS (DNA Cloning Service, Hamburg, Germany) was amplified from plasmid pFF_{19}eGFP (Timmermans *et al.*, 1990) using the eGFP ORF-PstI F and eGFP ORF-HindIII R primers and cloned into the pNOS-HvHOX2 promoter plasmid, which was then renamed *pNOS-ProHvHOX2::eGFP*. The same approach was followed for *pNOS-ProVRS1 (991bp)::HvHOX2* and *pNOS-ProVRS1 (991bp)::eGFP* constructs. All the above promoter–gene cassettes were then transferred from the pNOS (cloning) vector to the p6U (binary) (DNA Cloning Service) vector by non-directional cloning in the *Sfi*I site. The final plasmids were named according to the cassettes cloned into them. The resultant plasmids were also sequenced, and the integrity of the cloned fragments was verified. The selected binary plasmids were used to generate the stable transgenic barley plants (cv. Golden Promise) by *Agrobacterium*-mediated gene transfer following a method described previously (Hensel *et al.*, 2009). The basic cloning methods like PCR amplification, DNA electrophoresis, restriction digestion, ligation, and transformation into *Escherichia coli* were done according to standard procedures (Sambrook and Russell, 2001). All primers used for cloning are given in Supplementary Table S2.

Generation of Cas9 mutants

A synthetic double-stranded oligonucleotide carrying the protospacer sequence of the genomic target motif was inserted between the OsU3 promoter and the downstream gRNA scaffold present in a generic, monocot-compatible intermediate vector, pSH91 (Budhagatapalli *et al.*, 2016). Next, the whole expression cassette of gRNA-Cas9 was introduced into the *Sfi*I cloning site of the binary vector p6i-d35S-TE9 (DNA Cloning Service). The binary plasmid was used to obtain the stable transgenic barley plants (cv. Golden Promise) by *Agrobacterium*-mediated gene transfer following a method described previously (Hensel *et al.*, 2009).

Quantitative real-time PCR

The quantitative real-time PCR (qRT-PCR) was performed with gene-specific primers (mostly designed from the 3′-UTR) by using Power SYBR Green PCR Master Mix (Thermo Fisher Scientific) in an Applied Biosystems 7900HT Fast Real-Time PCR system (Thermo Fisher Scientific). The qRT primers were designed mostly by Primer3web (http://primer3.ut.ee/), and primers amplifying a fragment of 80–150 bp from the target cDNA were used. Genes like Serine/Threonine phosphatase PP2A catalytic subunit (HORVU4Hr1G074680) or Elongation factor-α (HORVU4Hr1G056740) were used to normalize the target amplicons between different tissues. A typical qRT-PCR reaction contained 5 µl of SYBR Green mix, 0.5 pmol of forward and reverse primers, and 1 µl of the template (dilution factor 2 or 4) in 10 µl reaction volume. The PCR was performed with the following thermal conditions: 50 °C for 2 min, 95 °C for 10 min, 40 cycles of 95 °C for 15 s and 60 °C for 1 min, and a final extension at 95 °C for 15 s. The homogeneity of amplicons was verified by the dissociation step at 60 °C for 15 s, followed by 95 °C for 15 s. Each sample was represented by three technical replicates and three biological replicates, and every qRT-PCR was repeated at least two times but mostly three times. The linearity of each PCR amplification was verified by LinRegPCR (Ruijter *et al.*, 2009), and reactions having a value ≥1.6 were taken for analysis. Relative expression levels of target genes were calculated by the $2^{-\Delta C_T}$ method or $\Delta\Delta C_T$ (Livak and Schmittgen, 2001), and the data were analysed by SDS 2.3 software (Thermo Fisher Scientific). The sequences of the primers used for qRT-PCR are provided in Supplementary Table S2. The qRT data were analysed using Prism software, version 8.4.2 (GraphPad Software, San Diego, CA, USA). Mean value comparison of different traits was made with multiple Student's *t*-tests, paired Student's *t*-test (parametric), and a one-way ANOVA with Tukey's multiple comparison test (α=5%).

Results

HvHOX1 *has higher nucleotide diversity compared with its paralog* HvHOX2

The eight natural alleles for *HvHOX1* known so far are grouped into two-rowed (*Vrs1.b2*, *Vrs1.b3*, *Vrs1.b5*, and *Vrs1.t1*) and six-rowed (*vrs1.a1*, *vrs1.a2*, *vrs1.a3*, & *vrs1.a4*) alleles (Komatsuda *et al.*, 2007; Sakuma *et al.*, 2017; Casas *et al.*, 2018). In contrast, the nucleotide diversity of *HvHOX2* is largely unknown. To fill this gap, we sequenced the *HvHOX2* promoter (1 kb) and gene (including 5′- and 3′-UTRs) in 83 diverse spring barleys (44 two-rowed and 39 six-rowed). Surprisingly, we found only four SNPs, restricted to the promoter (two SNPs), 5′-UTR (one SNP), and intron-2 (one SNP). At the same time, the CDS was identical and highly conserved in all these accessions (Supplementary Table S3). We further expanded our nucleotide diversity study by sequencing *HvHOX1* and *HvHOX2* in 24 *Hordeum* spp. (Supplementary Table S1), which showed the non-synonymous (K_a) and synonymous (K_s) substitution values of *HvHOX1* (K_a=0.028, K_s=0.049) and *HvHOX2* (K_a=0.008, K_s=0.051). The lower K_a value of *HvHOX2* indicates that *HvHOX2* has been well conserved among the *Hordeum* species (Supplementary Table S4). A comparison of the nucleotide diversity (π) of these two genes (*HvHOX1*, Chr.2H: 581356498-581377358; *HvHOX2*, Chr.2H: 139932435-139953386) in 200 domesticated barleys (Jayakodi *et al.*, 2020) confirmed the lower π of *HvHOX2* compared with *HvHOX1* (Supplementary Fig. S1A). This study also revealed two major haplotypes for the *HvHOX2* genic region (Supplementary Fig. S1B), whereas *HvHOX1* possesses multiple haplotypes that span the analysed region (Supplementary Fig. S1C). This difference in diversity might be due to their physical location—*HvHOX1* is in the distal end of the high recombining region of chromosome 2H, while *HvHOX2* is closer to the centromeric region on 2H (Supplementary Fig. S1A). Collectively, all the above results indicate that *HvHOX2* is highly conserved compared with its paralog *HvHOX1*.

HvHOX1 and HvHOX2 are functional HD-ZIP class I transcription factors

The HD-ZIP class I proteins HvHOX1 and HvHOX2 show a very high sequence identity between their homeodomain (89.3%) and leucine zipper (90%) motifs. However, there are several amino acid changes across the proteins with yet unknown consequences (Supplementary Fig. S2). In particular,

HvHOX1 lacks a putative AHA-like motif in its C-terminus, which was predicted to be an interaction motif with the basal transcriptional machinery (Arce *et al*., 2011; Capella *et al*., 2014) (Supplementary Fig. S2). All these similarities and differences pave the way to compare the functionality of these two proteins.

We assessed the dimerization properties of HvHOX1 and HvHOX2 with a BiFC assay. *HvHOX1* and *HvHOX2* were cloned into split-YFP vectors, creating N-terminal c-myc-nYFP and HA-cYFP fusions. The resulting plasmids were co-transformed with a CFP construct into Arabidopsis mesophyll protoplasts. The CFP was a transformation control, accumulating in the nucleus and cytoplasm. The detection of yellow fluorescence in all four combinations indicated that the HvHOX1 and HvHOX2 proteins could form homo- or heterodimers (Fig. 1A). The superimposed YFP channel (dimerization) on the CFP channel (strong nuclear signal) indicated that homo- or heterodimers of both proteins are localized in the nucleus (Fig. 1A), which agrees with the nuclear localization predicted for both proteins (Sakuma *et al*., 2013). A western blot analysis using antibodies directed against HA and c-myc epitopes confirmed that the proteins were expressed full-length and at similar levels (Fig. 1B).

Following this, we verified the DNA binding properties of HvHOX1 and HvHOX2 with an EMSA using the *in vitro* translated proteins and experimentally verified *HD-Zip* I *cis*-element from Sessa *et al*. (1993). A clear shift of protein–DNA bands (marked with ⋆) for both proteins, especially at higher concentrations, indicated binding to the *HD-Zip* I *cis*-element (Fig. 1C). Binding specificity was further evaluated by

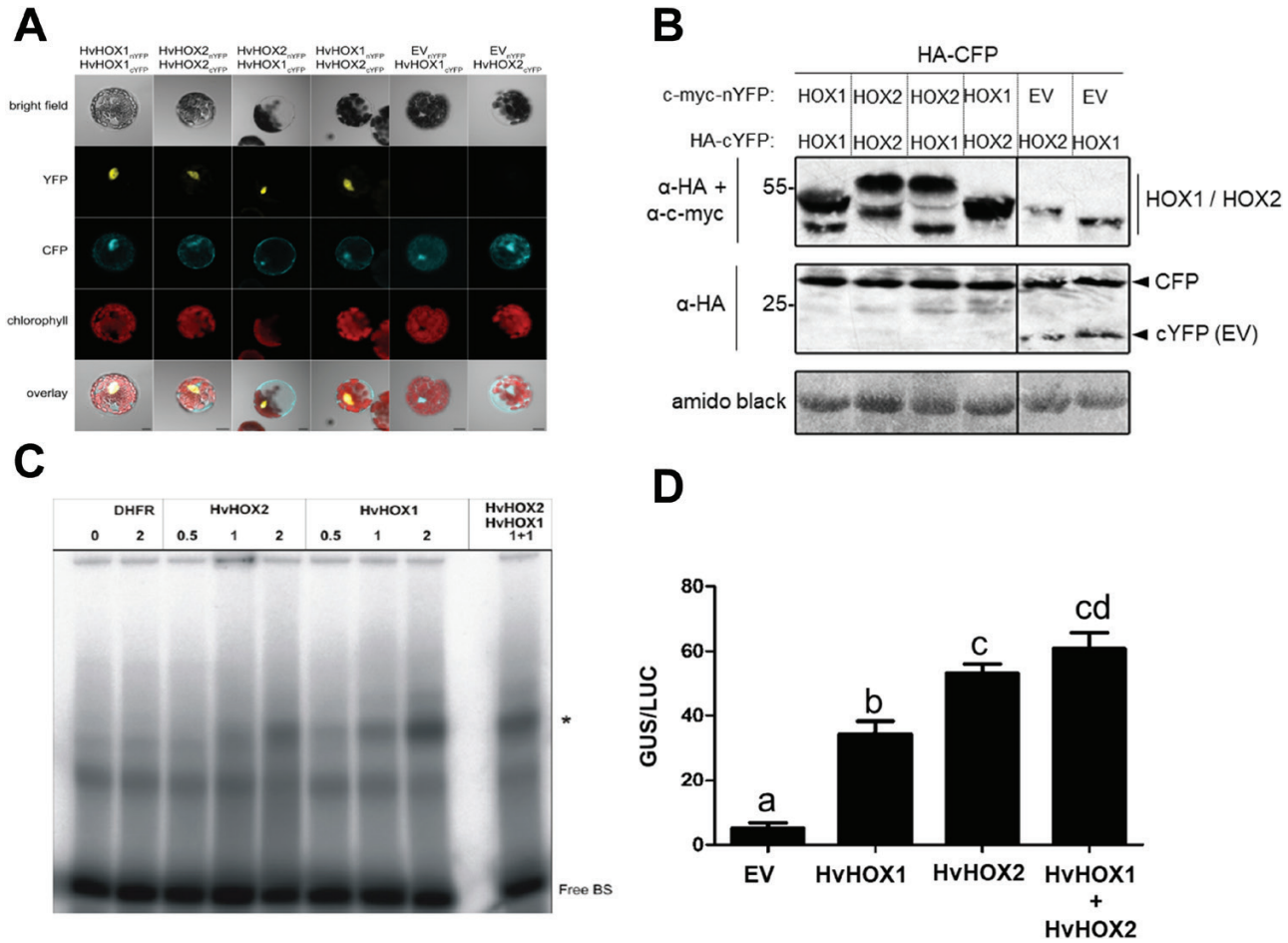

Fig. 1. HvHOX1 and HvHOX2 are functional HD-ZIP class I transcription factors. (A) Bimolecular fluorescence complementation (BiFC) assay for HvHOX1 and HvHOX2 proteins. The signal in the yellow fluorescent protein (YFP) panel indicates the dimer formation, and the cyan fluorescent protein (CFP) panel discloses the nucleus (blue, dark spot). The last overlay panel exhibits the localization of protein dimers in the nucleus. Scale bar: 10 µm. (B) Western blot for HvHOX1 and HvHOX2 proteins used for BiFC assay is shown. EV, empty vector; HA, hemagglutinin; c-myc, avian myelocytomatosis virus oncogene cellular homolog; 25 and 55 denote protein size in kilodaltons. (C) The specific binding of HvHOX1 and HvHOX2 proteins on HD-Zip I *cis*-element (BS, binding sequence) indicated with a star is shown by an EMSA. Dihydrofolate reductase (DHFR), negative control. Different numbers denote the protein volume in µl. (D) The transactivation property of HvHOX1 and HvHOX2 proteins is shown by the GUS activity relative to LUC. Data shown are means ±SE (n=3); letters above the bar indicate that the mean values are significantly different at the 1% probability level by one-way ANOVA with Newman–Keuls multiple comparison test. EV, empty vector; GUS, β-glucuronidase; LUC, luciferase.

competition assays with amplified DNA fragments of the targeted promoters. Here, we observed the binding of HvHOX1 to the *HvHOX2* promoter and mild interactions of HvHOX2 with the *HvHOX1* and *HvHOX2* promoters (Supplementary Fig. S3).

Next, we investigated these proteins' *in vivo* transactivation properties using a promoter GUS reporter system in Arabidopsis mesophyll protoplasts. We found that both proteins can transactivate a synthetic pGAL4-4×UAS::GUS reporter. Interestingly, the transactivation activity of HvHOX2 was significantly higher compared with that of HvHOX1 (Fig. 1D). Taken together, both HvHOX1 and HvHOX2 possess DNA binding activity, can form homo- or heterodimers, and have transactivation activities, which corroborate that they are functional HD-ZIP class I TFs.

Two-rowed cultivar Bowman's lateral spikelets have delayed differentiation and aborted reproductive organs

The size and fertility of lateral spikelets determine the row-type and intermedium-spike types in barley (Komatsuda *et al.*, 2007; Ramsay *et al.*, 2011; Youssef *et al.*, 2017; Zwirek *et al.*, 2019). To comprehend the differences between lateral and central spikelets in two-rowed barley, we tracked them from early initiation until pollination in the two-rowed cv. Bowman. Barley spike development starts from the double ridge (DR) stage, in which spikelet ridges are subtended by leaf ridges (Fig. 2A). In the next stage, known as 'triple mound' (TM), the spikelet ridge differentiates into one central (CSM) and two lateral (LSM) spikelet meristems, in which the CSM develops as a more prominent structure compared with the two LSMs (Fig. 2B). This marks the first developmental difference between the central and lateral spikelets. Following the TM stage, the CSM continues to differentiate into various spikelet/floret organ primordia (glume, lemma, palea, stamen, pistil, and awn) (Fig. 2C–F). However, the LSM exhibits a delayed differentiation from the glume primordium stage, indicating the suppression of LSM (Fig. 2C–F). At the awn primordium stage (AP), the central spikelets have completed the differentiation of all spikelet/floret organs, while the laterals have only achieved the differentiation of glume and lemma (Fig. 2F). We also compared the development of lateral spikelets between the two-rowed cv. Bowman and its near-isogenic six-rowed line BW-NIL(*vrs1.a*) (Druka *et al.*, 2011). Close to the white anther stage (Kirby and Appleyard, 1984), the difference between the laterals of two- and six-rowed spikes became apparent (Fig. 2G, H). The six-rowed laterals possessed primordia for all spikelet/floret organs, whereas the two-rowed laterals had retarded awn and pistil primordia (Fig. 2G, H). We also verified the divergence of lateral spikelet development in another pair of two- (cv. Bonus) and six-rowed (*hex-v.3*, *vrs1* deletion mutant) barleys (Supplementary Fig. S4).

To understand the sterility of lateral spikelets, we compared the histology of anther and pistil growth in Bowman and its *vrs1.a* mutant (BW-NIL(*vrs1.a*)) from Waddington stage 4.5 (W4.5, AP stage) to W10.0 (pollination)/W8.5 (Supplementary Figs S5, S6). The delayed differentiation of lateral spikelets observed during the spikelet initiation stages (TM to AP) continued in the growth stages of the reproductive organs. Anthers of two-rowed lateral spikelets showed an impeded differentiation (Supplementary Video S1) compared with the anthers of other spikelets (Supplementary Fig. S5A3–J3). However, the central spikelet anthers of two- (Supplementary Fig. S5A1–J1; Supplementary Video S1) and six-rowed (Supplementary Fig. S5A2–J2) exhibited an advanced progression rate across the stages. Notably, the six-rowed lateral anther (Supplementary Fig. S5A4–J4) followed a differentiation rate between the two- and six-rowed centrals as well as the two-rowed laterals, indicating that there are additional suppressors of lateral spikelet development besides HvHOX1. Moreover, anthers of the two-rowed lateral spikelets stopped differentiation at W7.5 (Supplementary Fig. S5E3), followed by tissue disintegration in the subsequent stages (Supplementary Fig. S5E3–J3). In contrast, all other anthers continued their growth towards pollination (Supplementary Fig. S5). A similar delay of differentiation and disintegration of tissues was also observed in the pistil of two-rowed laterals at W7.5 (Supplementary Fig. S6C5). These results substantiate that two-rowed spikes have delayed lateral spikelet initiation and suppressed growth compared with their central spikelet.

HvHOX1 *and* HvHOX2 *have contrasting levels of expression during spikelet initiation and growth*

To evaluate the contribution of *HvHOX1* and *HvHOX2* across the spikelet developmental stages, we reanalysed the expression values of *HvHOX1* and *HvHOX2* from the Bowman RNA-seq spike atlas data (Thiel *et al.*, 2021) (Fig. 3A–C). In the whole spike, both genes showed a linear increase in expression along with the spikelet initiation stages (Fig. 3A). Except for the DR stage, *HvHOX1* generally displayed higher transcript levels than *HvHOX2* (TM to AP). This was particularly evident in glume primordium (GP), lemma primordium (LP), and stamen primordium (SP) stages (Fig. 3A). Similarly, in central and lateral spikelets, *HvHOX1* showed significantly higher expression level than *HvHOX2* in the SP stage of central and at several stages (TM, LP, and SP) of lateral spikelets (Fig. 3B, C). The high expression of *HvHOX1* in the laterals correlates with the delayed differentiation and suppression of the lateral spikelets (compared with the centrals) from the TM to AP stages in Bowman. These data are in line with the hypothesis that HvHOX1 acts as a negative regulator of lateral spikelet development in barley (Komatsuda *et al.*, 2007; Sakuma *et al.*, 2010, 2013). The presence of *HvHOX1* transcripts in central spikelets of two-rowed barleys, which are fertile and do not show any developmental disorder, poses a question that has yet to be

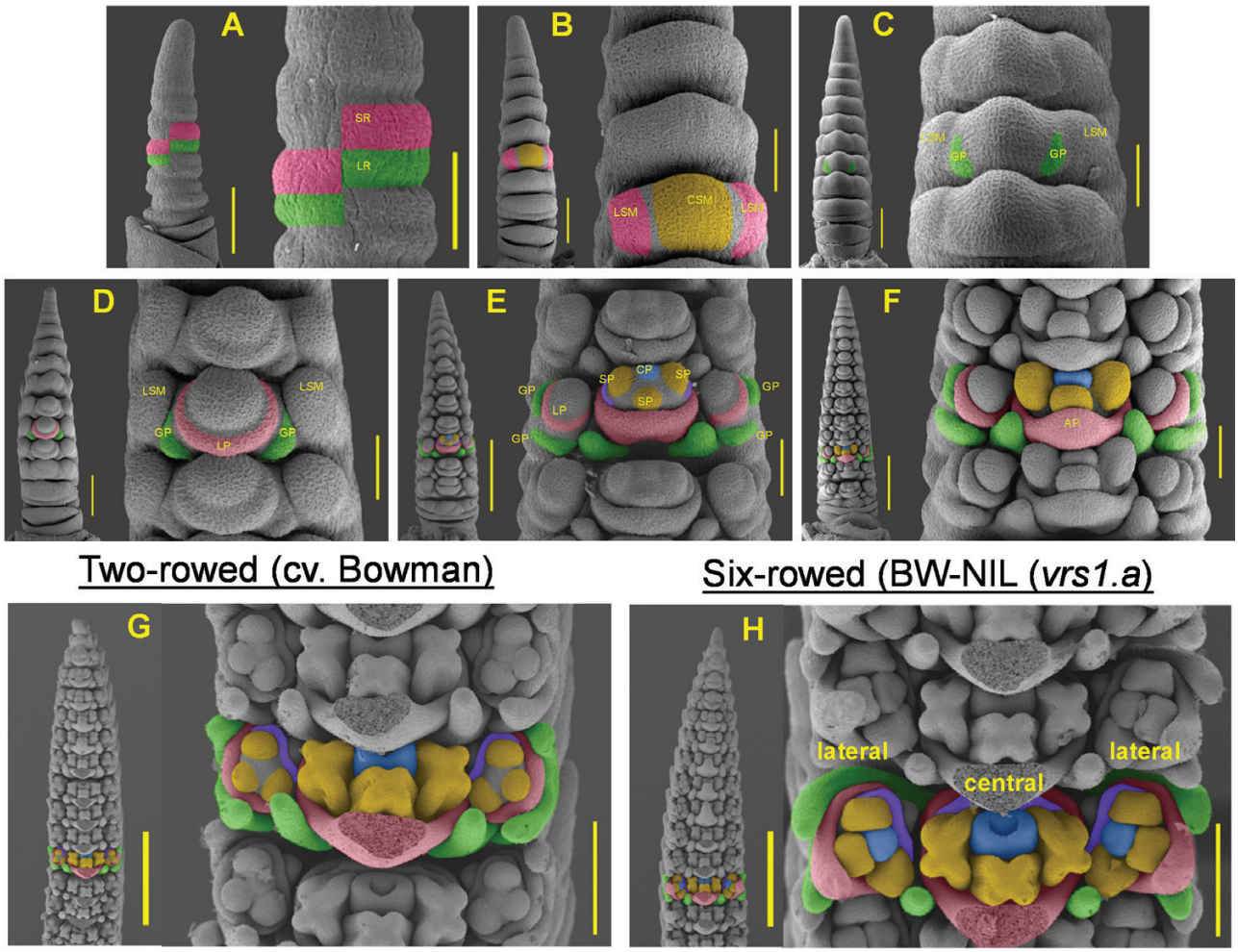

Fig. 2. Two-rowed spikes have delayed and reduced lateral spikelet development compared with its central and six-rowed lateral spikelets. (A–F) A series of early spike developmental stages of two-rowed cv. Bowman is shown: (A) Double ridge (DR); (B) triple mound (TM); (C) glume primordium (GP); (D) lemma primordium (LP); (E) stamen primordium (SP); and (F) awn primordium (AP). (G, H) A comparison of the Waddington (W) 5.5-stage spike of the two-rowed Bowman and its six-rowed mutant BW-NIL(*vrs1.a*) shows that the lateral spikelet organs of Bowman (G) are reduced and delayed compared with the mutant (H). Scale bar in (A): whole spike, 500 µm; magnified three nodes, 100 µm; (B, C): 500 µm and 200 µm; (D) 500 µm and 100 µm; (E, F) 200 µm and 100 µm; (G, H) whole spike, 800 µm; magnified three nodes, 200 µm.

solved (Komatsuda *et al.*, 2007; Sakuma *et al.*, 2010, 2013) (Fig. 2C–F, Supplementary Figs S5, S6).

Next, we analysed expression levels of these genes in the spikelet growth stages of Bowman and BW-NIL(*vrs1.a*) (non-functional *HvHOX1*) by qRT-PCR in the whole spike (W5.0, W5.5, and W6.0) and central and lateral spikelets (W7.5, W8.5, and W10.0) (Fig. 3D–I). Also, in these stages, *HvHOX1* exhibited significantly higher expression than *HvHOX2* in the whole spike at W5.0, W5.5, and W6.0, both in Bowman and BW-NIL(*vrs1.a*) (Fig. 3D, G). At later stages (W7.5 to W10.0), expression levels were inverted in both genotypes in central spikelets. *HvHOX2* transcripts accumulated to significantly higher levels at several stages (Fig. 3E, H). Interestingly, in the lateral spikelets, contrasting expression patterns were measured in both genotypes. In Bowman, *HvHOX1* transcript levels were significantly higher than *HvHOX2* levels in stages W7.5 and W8.5 but not W10.0. Meanwhile, in BW-NIL(*vrs1.a*), stages W7.5 and W8.5 did not show a difference between the two genes, but in stage W10.0, *HvHOX1* levels were significantly higher.

Promoters of HvHOX1 *and* HvHOX2 *share similar spatiotemporal expression patterns during spike growth stages*

The expression studies of *HvHOX1* and *HvHOX2* (Fig. 3A–I) exemplified that these genes have similar temporal expression patterns during the spikelet initiation and growth stages, though at different amplitudes. Additionally, their central- and lateral-specific transcript levels indicated they might share spatial boundaries across the initiation and growth stages. To verify their spatial co-localization and similar temporal expression

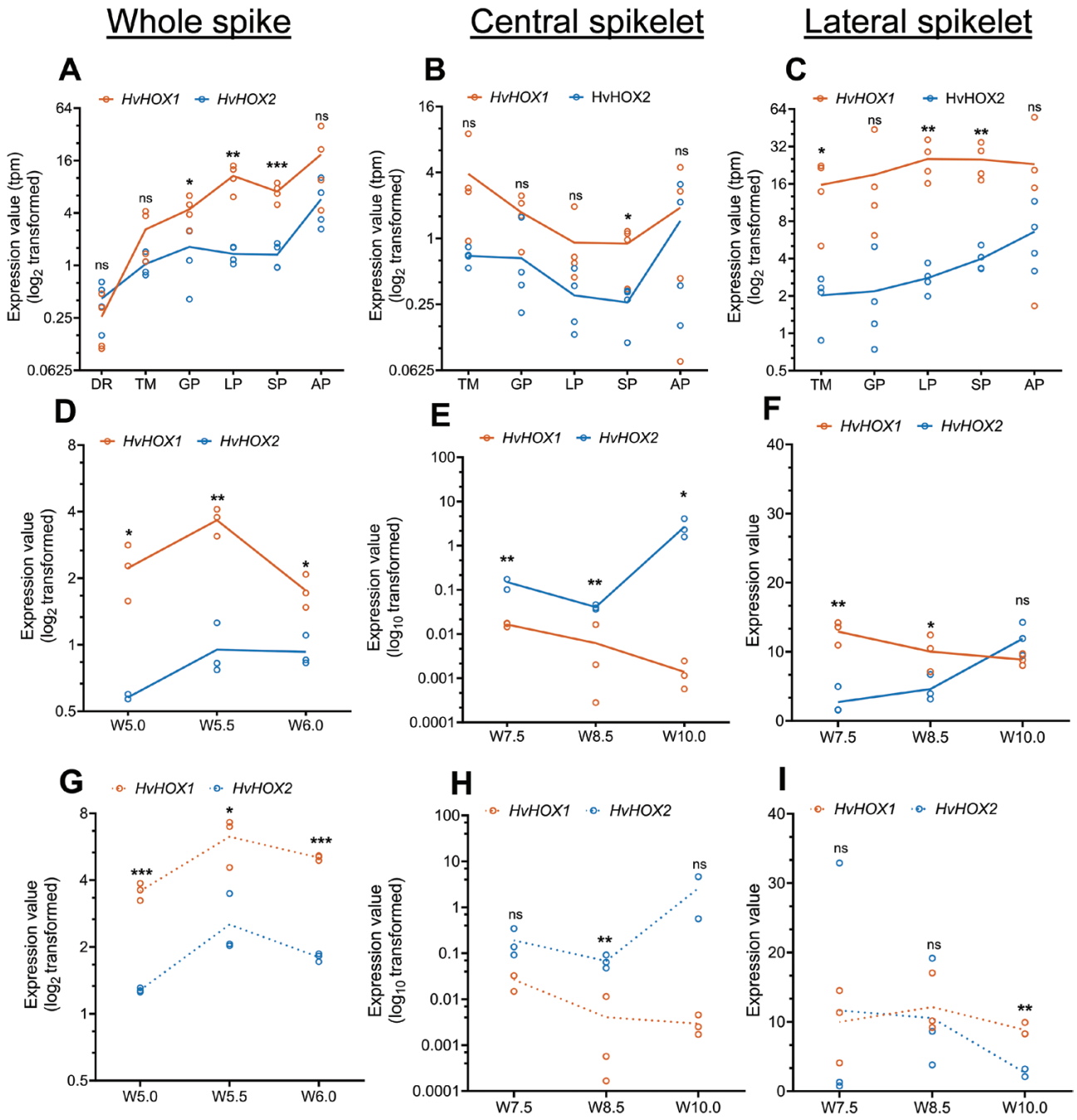

Fig. 3. *HvHOX1* and *HvHOX2* expression patterns during spike development. (A–C) The expression patterns of *HvHOX1* and *HvHOX2* genes in the whole spikes (A), central spikelets (B), and lateral spikelets (C) during early spike developmental stages. (D–I) Expression variation of *HvHOX1* and *HvHOX2* genes in the whole spike (D, G), central spikelet (E, H), and lateral spikelet (F, I) of Bowman and BW-NIL(*vrs1.a*) during later spike developmental stages, respectively. Mean values are compared with multiple Student's *t*-tests; **P*<0.05, ***P*<0.01, ****P*<0.001, mean values are significantly different; ns, not significantly different.

patterns, promoters (*HvHOX2*, 1929 bp; *HvHOX1*, 991 bp) of these genes were fused with a synthetic *GFP* coding sequence and transformed into the two-rowed cv. Golden Promise. Five and eight independent transgenic events showed GFP accumulation in the T_0 generation for *HvHOX1* and *HvHOX2* GFP constructs, respectively. Three independent events from both constructs were selected, and their GFP accumulation was confirmed until the T_2 generation. We found promoter activity of these genes in identical tissues like the central spikelet's carpel and anther (Fig. 4A, D), the tapetal layer of the central spikelet's anther (Fig. 4B, E), and rudimentary lateral anthers (Fig. 4C, F) at the W8.5 stage. Interestingly, we found

the promoter activity of only *HvHOX1* during the early spike developmental stages but not of *HvHOX2* (Supplementary Fig. S7). This could be due to the generally lower expression of *HvHOX2* at early stages (Fig. 3A) or the promoter used in this study is missing *cis*-elements responsible for early expression. It is important to note that the *in situ* expression of *HvHOX2* was also found at later (white anther, ~≥W6.0) stages of development in another study (Sakuma *et al.*, 2013). Together, the tissue-specific expression analyses and the promoter activity in the transgenic plants suggested that *HvHOX1* and *HvHOX2* might have partially similar spatiotemporal expression patterns during spikelet growth stages.

HvHOX1 *and* HvHOX2 *are ancestrally related and potentially play a similar role in spikelet development*

We constructed co-expression signatures of *HvHOX1* and *HvHOX2* genes from the transcript profiles across six spikelet initiation and growth stages (W2.5, W3.0, W4.5, W6.5, W7.5, and W8.5) in Bowman. We found 20 co-expression modules from a set of 7520 genes that showed a dynamic expression profile (Fig. 4G, H). *HvHOX1* and *HvHOX2* genes clustered together in one module (Fig. 4G; red) along with 4213 genes. A weighted gene co-expression network analysis revealed that *HvHOX1* shares one part of its co-expression module (Fig. 4I, shown in blue, 16 genes) with *HvHOX2*, while *HvHOX1* has unique co-expressed signatures (Fig. 4I, shown in orange, 39 genes). Most importantly, *HvHOX2* is one of the co-expressed genes within the *HvHOX1* module (Fig. 4I), which indicates that *HvHOX2* may also play the same role as *HvHOX1* in barley spikelet development. These data also suggest that both genes share a similar expression signature across spike development, and they support our previous transcript and GFP analyses. Furthermore, hierarchical clustering divided the genes within the shared module (Supplementary Fig. S8A; blue module from Fig. 4I) into two sub-clusters based on their expression in central and lateral spikelets, but not the unique *HvHOX1* co-expressed module (Supplementary Fig. S8B; orange module from Fig. 4I). The shared module was enriched with genes (e.g. *AGAMOUS* (*AG*), *SUPPRESSOR OF OVEREXPRESSION OF CONSTANS 1* (*SOC1*), *ENOLASE 1* (*ENO1*), and *AUXIN F-BOX PROTEIN 5* (*AFB5*)) associated with flower development, promotion of flowering, pistil/carpel and stamen identity, auxin signaling, transcription, and nitrate assimilation (Covington and Harmer, 2007; Dreni and Kater, 2014; Hyun *et al.*, 2016; Gaufichon *et al.*, 2017). This suggests that both HvHOX1 and HvHOX2 may promote spikelet/flower development. The *HvHOX1* unique co-expressed module was enriched in genes (such as *BREVIPEDICELLUS 1* (*BP1*), *WRKY 12*, *NOVEL PLANT SNARE 11* (*NPSN11*), *FORMIN HOMOLOGY 14* (*AFH14*), *LONELY GUY 3* (*LOG3*), and *G PROTEIN ALPHA SUBUNIT 1* (*GPA1*)) that are predicted to be involved in inflorescence architecture, flower development, ABA response, cell division, cell communication, senescence, and cell death (Li *et al.*, 2010; Tokunaga *et al.*, 2012; Zhao *et al.*, 2015; Li *et al.*, 2016; Chakraborty *et al.*, 2019; Wu *et al.*, 2020) (Supplementary Table S5). These genes support the rather suppressive role of HvHOX1 during barley spikelet development. Thus, our co-expression network study indicates that *HvHOX1* and *HvHOX2* are ancestrally related homeobox genes that may play a similar role in barley spikelet development.

HvHOX2 is dispensable for barley spikelet development

To validate the contribution of HvHOX1 and understand the function of HvHOX2, we developed *Hvhox1* and *Hvhox2* mutants by CRISPR/Cas9-mediated gene editing. A guide RNA was designed for the conserved homeodomain region shared by *HvHOX1* and *HvHOX2* for site-directed mutagenesis of both genes (Fig. 5A). We created the mutants in the two-rowed cv. Golden Promise, via stable transformation, using respective constructs and identified two independent events (E02 and E07) bearing different insertions and/or deletions by sequencing their target regions (Fig. 5A). Among the progenies of these primary mutants (heterozygous/biallelic), wild-type (T-DNA-free, non-mutant) plants, as well as single and double mutants for both genes, were selected. For *Hvhox1*, the respective one- or eight-nucleotide deletions in the E02_*Hvhox1* and E07_*Hvhox1* mutants (Fig. 5A) resulted in frame-shifted HvHOX1 proteins after position F75 within the homeodomain (Supplementary Fig. S9A, B). Regarding *Hvhox2*, the E02_*Hvhox2* event had a seven-nucleotides addition and four-nucleotides deletion (Fig. 5A), the latter resulting similarly in a frameshift after the corresponding F74 of the HvHOX2 protein (Supplementary Fig. S9D) while the former caused a replacement of F74 by RW within the homeodomain (Supplementary Fig. S9C). Comparison of spikelet development in these mutants at W4.5 and after spike maturity revealed that the central and lateral spikelets of the *Hvhox2* mutants (Fig. 5C; Supplementary Fig. S10B) displayed a similar stage of differentiation as in the spikes of wild-type plants (Fig. 5B; Supplementary Fig. S10A). Analogous to the pattern of spikelet differentiation, the matured spikes of *Hvhox2* mutants (Fig. 5G; Supplementary Fig. S10F) possessed smaller (compared with the centrals) and sterile lateral spikelets like in spikes of wild-type plants (Fig. 5F; Supplementary Fig. S10E), implying that *HvHOX2* might not suppress spikelet primordia differentiation and growth. However, *Hvhox1* single (Fig. 5D; Supplementary Fig. S10C) and double mutants (*Hvhox1–Hvhox2*) (Fig. 5E; Supplementary Fig. S10D) exhibited advanced lateral spikelet differentiation compared with wild-type plants (Fig. 5B; Supplementary Fig. S10A) and *Hvhox2* mutants (Fig. 5C; Supplementary Fig. S10B).

Interestingly, the lateral spikelet differentiation of *Hvhox1* (Fig. 5D; Supplementary Fig. S10C) and double mutants (*Hvhox1–Hvhox2*) (Fig. 5E; Supplementary Fig. S10D) was at a

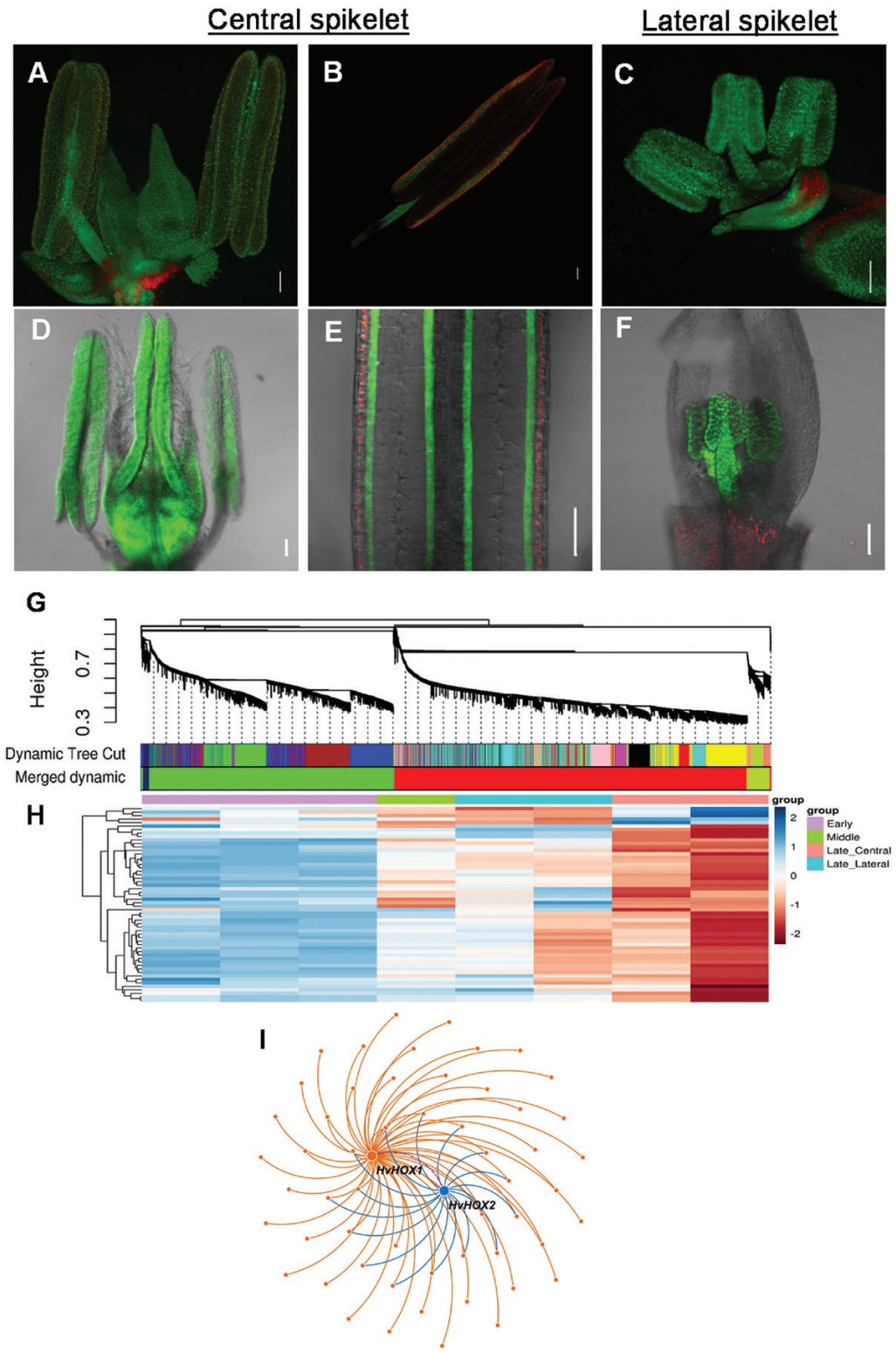

Fig. 4. Spatiotemporal expression patterns of *HvHOX1* and *HvHOX2* and their network of co-expressed genes during spike growth and development. (A–C) *HvHOX1* promoter activity (GFP expression) in central spikelets' stamen and pistil (A), tapetum and filament of stamen (B), and lateral spikelet's stamen (C) at Waddington 8.5 stage. (D–F) Similarly, *HvHOX2* promoter activity in the central spikelet's stamen and pistil (D), tapetum of an anther (E), and lateral spikelets' stamen (F). Green color, GFP fluorescence; red color, chlorophyll autofluorescence. Scale bar: 100 μm. Modules of the co-expressed genes were assigned colors, shown by the horizontal bars below the dendrogram. (G) Merged modules are shown under the dynamic module profile. (H, I) The expression (log_2 normalized value) heat map of the red module (H) and the co-expressed gene clusters (I) of *HvHOX1* and *HvHOX2*.

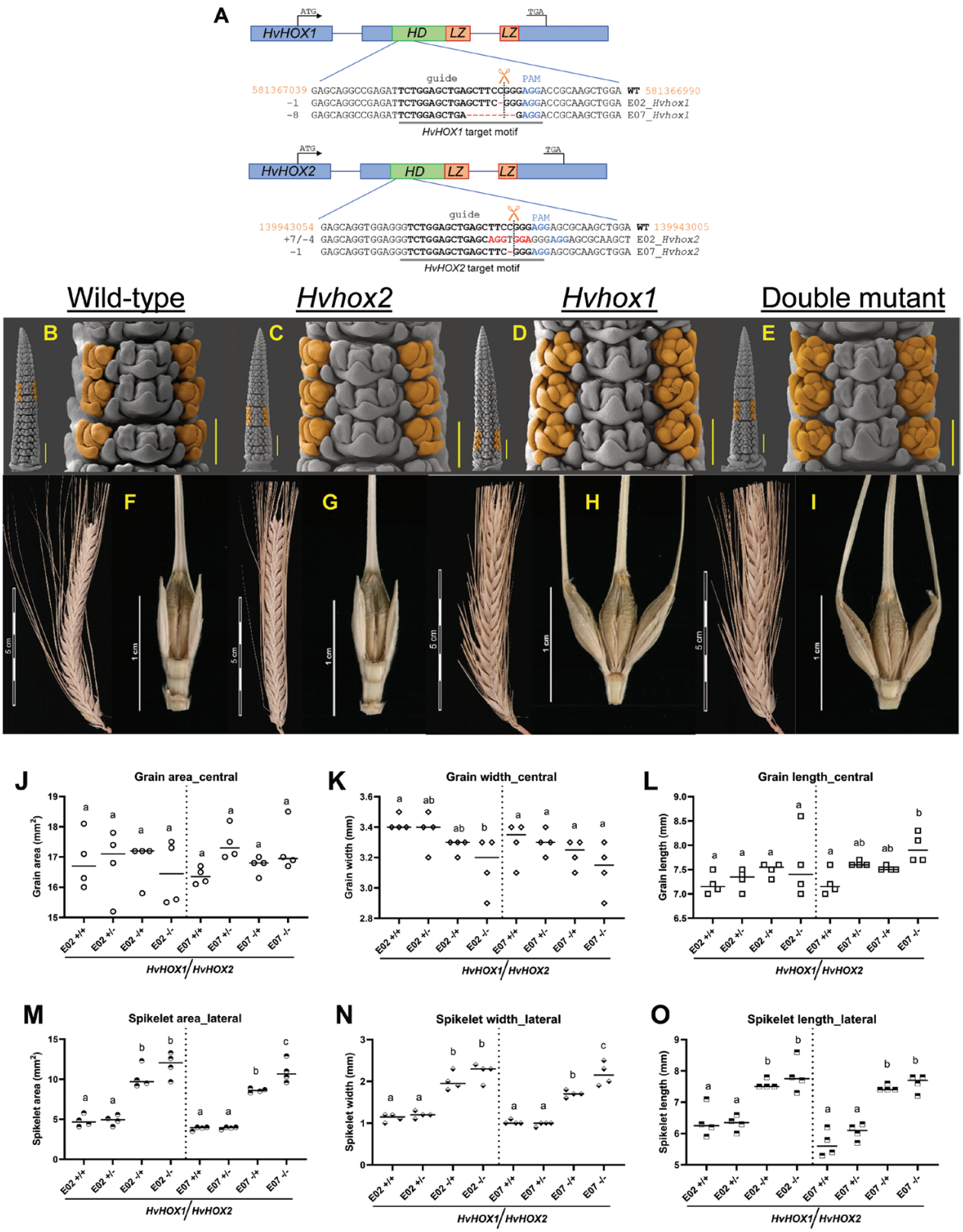

Fig. 5. The HvHOX2 is dispensable for barley spikelet development. (A) The guide sequences used to generate the mutants and the mutated nucleotide sequences of two mutants of *HvHOX1* and *HvHOX2* genes by CRISPR are shown. (B–I) Images representative of E07 mutants. A comparison of immature (B–E) and mature (F–I) spikes reveals that the wild-type (null transgenic) (B) and *Hvhox2* (C) immature spikes have a much delayed lateral

spikelet development compared with the *Hvhox1* single (D) and *Hvhox1–Hvhox2* double (E) mutants. (F–I) Similarly, the wild-type (null transgenic) (F) and *Hvhox2* (G) mature spikes have sterile lateral spikelets (without grain formation), while the *Hvhox1* single (H) and *Hvhox1–Hvhox2* double (I) mutants' spikes possess fertile lateral spikelets or grains. Scale bar: (B–E) whole spikes, 500 µm; magnified three nodes, 200 µm. HD, homeodomain; LZ, leucine zipper. (J–O) Grain or spikelets' area, width, and length of central (J–L) and lateral (M–O) of wild-type, single and double mutants of *HvHOX1* and *HvHOX2*. Mean values (J–O) are compared with one-way ANOVA with Tukey's multiple comparison test; different letters denote the values are significantly different at 5% probability levels, and the same letter shows that they are not significantly different.

similar stage at W4.5, which reiterated the fact that *HvHOX1* suppresses lateral spikelet development in two-rowed spikes, irrespective of the function of *HvHOX2*. As expected, spikes of *Hvhox1* single (Fig. 5H, Supplementary Fig. S10G) and double (*Hvhox1–Hvhox2*) mutant (Fig. 5I; Supplementary Fig. S10H) had bigger and fertile spikelets (grains) like six-rowed barley. Grain morphometric measurements confirmed the above results and showed that *Hvhox2* mutants did not show a significant difference for any of the traits compared with the wild-type (Fig 5J–O). However, the lateral spikelets' area, width, and length of *Hvhox1* single and double mutants were significantly higher than the wild-type and *HvHOX2* mutants (Fig. 5M–O).

Independently, we screened the *HvHOX2* CDS in 5500 second-generation (M_2) TILLING mutant lines of cv. Barke (Gottwald *et al.*, 2009) and found only four mutations. Among these, three were synonymous, and one was a non-synonymous (P197S, line 11869) nucleotide substitutions (Supplementary Fig. S11). The mutant line 11869 did not show aberrations during spike development and growth in the M_3 generation, which supported our CRISPR/Cas9 *Hvhox2* mutants. Combining these results suggested that HvHOX2 is not essential for barley spikelet development and growth despite its evolutionary conservation.

Discussion

HvHOX1 and HvHOX2 are two functional HD-ZIP class I transcription factors that are ancestrally related

Based on the sequence similarity of orthologs within grass species, it was proposed that HvHOX2 might have a similar molecular function in the Poaceae (Sakuma *et al.*, 2010). However, *HvHOX1*, specific to the Triticeae tribe, showed a very high sequence variation, at least in barley (Komatsuda *et al.*, 2007; Saisho *et al.*, 2009; Casas *et al.*, 2018). *HvHOX1* and *HvHOX2* are duplicated genes, for which it was hypothesized that *HvHOX2* might have retained the ancestral sequence and promotion of development, while *HvHOX1* became neofunctionalized as a suppressor of lateral spikelets (Sakuma *et al.*, 2010, 2013). Our nucleotide diversity study supports this postulation, as we found a higher nucleotide diversity for *HvHOX1* than *HvHOX2* (Supplementary Fig. S1; Supplementary Table S4). Despite a few amino acid changes between HvHOX1 and HvHOX2 proteins (Supplementary Fig. S2), both can bind to the HD-ZIP class I-specific *cis*-element, make dimers, and transactivate their downstream genes (Fig. 1; Supplementary Fig. S3), thus, confirming that both are functional HD-ZIP class I TFs. It is known that HD-ZIP TFs only bind to DNA as dimers (Sessa *et al.*, 1993). Our transactivation study showed that the HvHOX2 homodimers have stronger transactivation activity than the HvHOX1 homodimers (Fig. 1D), which might be caused by the missing putative AHA-like motif in the C-terminus of HvHOX1 (Supplementary Fig. S2). This motif was predicted to be an interaction motif with the basal transcriptional machinery (Arce *et al.*, 2011; Capella *et al.*, 2014). Interestingly, the HvHOX1–HvHOX2 heterodimer transactivation was significantly higher than that of the HvHOX1 homodimer, indicating that heterodimers of HD-ZIP class I TFs might have stronger transactivation potential than the homodimers as shown recently with two HD-ZIP class I TFs in lily (*Lilium longiflorium*) (Wu *et al.*, 2024). Although our expression studies suggested that both genes have similar temporal (Fig. 3) and spatial (Fig. 4A–F) expression patterns during spikelet initiation and growth stages, we observed significant differences in the transcript levels of the two genes in the early spikelet development and later growth stages (Fig. 3). This could be due to the *HvHOX1*'s upstream regulator HvRA2, which expresses both in lateral and in central spikelets like *HvHOX1* (Koppolu *et al.*, 2013). Our gene co-expression network analysis revealed that, most likely, these genes share similar gene networks, as they fall into the same cluster of co-expressed genes and share a common network of genes (Fig. 4G–I). This finding reaffirms the hypothesis that both genes have originated from a common ancestral gene (Sakuma *et al.*, 2010, 2013). Crucially, *HvHOX1* has a unique network of genes (Fig. 4I) that are highly expressed in lateral spikelets (Supplementary Fig. S8B) and are involved in the suppression of development and exerting cell death (Supplementary Table S5) (Thirulogachandar *et al.*, 2017). This is in line with the hypothesis that HvHOX1 acts as a suppressor of development and growth regardless of in which tissue it is expressed in barley. Additionally, our analyses of differentially expressed genes between Bowman and BW-NIL(*vrs1.a*) (Supplementary Figs S12, S13) supported the suppressive role of HvHOX1 on barley lateral spikelet development. However, the shared network genes of *HvHOX1* and *HvHOX2* are expressed in the central and lateral spikelets and predicted to promote development and flowering. This indicates that both may have similar functions.

HvHOX1 is a suppressor of, while the paralogous HvHOX2 is dispensable for, spikelet development

HvHOX1 was previously proposed as a suppressor of lateral spikelet, specifically pistil development, in barley (Komatsuda

et al., 2007; Sakuma et al., 2010, 2013). HvHOX2, on the contrary, was proposed to promote spike development in barley (Sakuma et al., 2010, 2013). We generally found *HvHOX1* and *HvHOX2* to be expressed throughout spike development. Interestingly, we observed an increase in the expression of both genes during early spike developmental stages (Fig. 3A). Mostly, *HvHOX1* transcripts accumulated to significantly higher levels. In addition, we found delayed meristem differentiation (Fig. 2B–F) and suppressed anther and pistil development within the lateral spikelets (Supplementary Figs S5, S6; Supplementary Video S1). Together, these data correlate with the suppressor hypothesis for HvHOX1. Nevertheless, we also detected *HvHOX1* transcript accumulation in central spikelets during early and late development (Fig. 3B, E). However, we observed no disorder during central spikelet differentiation (Fig. 2B–G) or growth of reproductive organs (Supplementary Figs S5, S6) in two-rowed barley. Also, previous studies did not report any developmental irregularities in central spikelets of two-rowed barley (Komatsuda et al., 2007; Sakuma et al., 2010, 2013; Zwirek et al., 2019). We, therefore, hypothesized that this could be due to a lower level of *HvHOX1* transcripts (compared with the laterals) (Fig. 3B, E) and some positive regulators, which act antagonistically to HvHOX1 in central spikelets, or HvHOX1 has a dual role, i.e. it works as a promotor in central and suppressor in the lateral spikelets.

Our CRISPR/Cas9 mutant study clearly showed that HvHOX2 is not essential during barley spikelet development because the two *Hvhox2* mutants retained a canonical spikelet development in laterals and centrals similar to wild-type plants (Fig. 5; Supplementary Fig. S10). However, *Grassy Tillers1* (*HvGT1*), a homolog of *HvHOX1* and *HvHOX2*, might have a redundant function and compensate for *HvHOX2*'s absence in the *Hvhox2* mutants (gene compensation) (El-Brolosy et al., 2019; Ma et al., 2019; Peng, 2019). *HvGT1* is expressed in both central and lateral spikelets during the early spikelet development stages (Supplementary Fig. S14), and we have recently shown that HvGT1 suppresses apical spikelet development in barley (Shanmugaraj et al., 2023). Also, in maize and brachypodium, GT1 and HvHOX1 (VRS1) homologs repress floral organs (Gallagher et al., 2023). Indeed, this hypothesis requires further validation, which we will address in the future by generating double and triple mutants of *HvHOX1*, *HvHOX2*, and *HvGT1*. Since HD-ZIP TFs can form homo- and heterodimers with other HD-ZIP TFs (Johannesson et al., 2001; Wu et al., 2024), another possibility could be that the transcriptional activity of HvHOX1 and HvHOX2 might be fine-tuned by the formation of developmental and/or tissue-specific homo- and/or hetero-dimers influenced by the expression level of HD-ZIP TFs. This hypothesis can be addressed by a tissue-specific overexpression of HD-ZIP TFs (*HvHOX1*, *HvHOX2*, and *HvGT1*). Interestingly, ubiquitous overexpression of orthologous *HOX2* genes in wheat (Wang et al., 2017) and rice (Shao et al., 2018) reduced the inflorescence length and complexity, which suggested a potential suppressive role in inflorescence development, at least in other grasses. Thus, our expression and transgenic studies show that *HvHOX1* plays a suppressive role during barley lateral spikelet development, while its paralog *HvHOX2* might act redundantly to some extent but most likely has evolved differently.

Supplementary data

The following supplementary data are available at *JXB* online.

Fig. S1. Comparison of *HvHOX1* and *HvHOX2* nucleotide diversity in 200 domesticated barleys.

Fig. S2. Pairwise alignment of HvHOX1 and HvHOX2 proteins.

Fig. S3. EMSA competition assay of *in vitro* translated HvHOX1 and HvHOX2.

Fig. S4. Two-rowed spikes have delayed lateral spikelet development compared with its central spikelet and six-rowed lateral spikelets.

Fig. S5. Transverse sections of anthers from central and lateral spikelets of Bowman and BW-NIL(*vrs1.a*).

Fig. S6. Transverse sections of carpels from central and lateral spikelets of Bowman and BW-NIL(*vrs1.a*).

Fig. S7. *HvHOX1* promoter activity in early spike development stages.

Fig. S8. Hierarchical clustering of *HvHOX1* and *HvHOX2* shared and *HvHOX1* unique modules.

Fig. S9. Sequence alignment of the wild-type and mutant proteins of HvHOX1 and HvHOX2 resulting from the CRISPR/Cas9 study.

Fig. S10. The HvHOX2 is dispensable for barley spikelet development.

Fig. S11. Multiple sequence alignment of the orthologous HvHOX2 proteins and HvHOX2 from a TILLING mutant 11869.

Fig. S12. Gene ontology of differentially expressed genes in W2.5, W3.0, and W4.5 in Bowman and BW-NIL(*vrs1.a*).

Fig. S13. Gene ontology of differentially expressed genes in W7.5 and W8.5 lateral spikelets of Bowman compared with BW-NIL(*vrs1.a*).

Fig. S14. Expression of barley *Grassy Tillers1* in the central and lateral spikelets during early spikelet development stages.

Table S1. List of *Hordeum* species used in this study.

Table S2. Primers used in this study.

Table S3. *HvHOX2* SNP haplotypes identified in 83 diverse spring barley collection.

Table S4. Nucleotide diversity of *HvHOX1* and *HvHOX2* in *Hordeum* species.

Table S5. List of genes co-expressed with *HvHOX1* and *HvHOX2* genes during spike development in cv. Bowman.

Video S1. Comparison of a two-rowed lateral and central spikelet development around W8.0.

Acknowledgements

We sincerely thank Jana Lorenz, Mandy Püffeld, Gabi Einert, Corinna Trautewig, and Angelika Püschel for their excellent technical support. We would like to thank Karin Lipfert, Heike Müller, Gudrun Schütze, and Andreas Bähring for their photography and graphical work. We are grateful to Sabine Sommerfeld and Sibylle Freist for technical assistance in barley transformation. We also extend our thanks to Prof. Nils Stein for providing access to the TILLING screening platform.

Author contributions

VT, NS, TS, GG, and TK conceptualized the study. NS, TS, and MK supervised the study. VT, and TR performed microscopic analyses. VT and GG generated transcriptome data;VT and SK analysed the transcriptome data. GH and JK generated transgenics and targeted gene-specific mutants; and VT analysed the mutants. JR molecularly characterized CRISPR mutants. RK, TS, SS, TK, and MJ performed resequencing of genes and TILLING analysis. GG,VT, PSR, and CS prepared constructs for protein characterization. L.E-L., GG, and JL conducted transactivation and BiFC experiments, and MK performed DNA binding study (EMSA). VT compiled and interpreted all the data and drafted the manuscript. All the authors reviewed the manuscript.

Conflict of interest

The authors declare no conflict of interest.

Funding

The work in NS's lab was supported by IZN (Interdisciplinary Centre for Crop Plant Research), Halle (Saale), Saxony-Anhalt, Germany. The work in TS's lab was supported by the European Research Council (ERC), grant agreement 681686 'LUSH SPIK0045', ERC-2015-CoG; HEISENBERG Program of the German Research Foundation (DFG), grant no. SCHN 768/15-1; and the IPK core budget.

Data availability

The transcriptomic data used in this study are deposited in the public repository e!DAL, and it can be accessed with this link: http://dx.doi.org/10.5447/ipk/2021/20

References

Arce AL, Raineri J, Capella M, Cabello JV, Chan RL. 2011. Uncharacterized conserved motifs outside the HD-Zip domain in HD-Zip subfamily I transcription factors; a potential source of functional diversity. BMC Plant Biology **11**, 42.

Bonnett OT. 1935. The development of the barley spike. Journal of Agricultural Research **51**, 451–457.

Budhagatapalli N, Schedel S, Gurushidze M, *et al*. 2016. A simple test for the cleavage activity of customized endonucleases in plants. Plant Methods **12**, 18.

Bull H, Casao MC, Zwirek M, *et al*. 2017. Barley *SIX-ROWED SPIKE3* encodes a putative Jumonji C-type H3K9me2/me3 demethylase that represses lateral spikelet fertility. Nature Communications **8**, 936.

Capella M, Re DA, Arce AL, Chan RL. 2014. Plant homeodomain-leucine zipper I transcription factors exhibit different functional AHA motifs that selectively interact with TBP or/and TFIIB. Plant Cell Reports **33**, 955–967.

Casas AM, Contreras-Moreira B, Cantalapiedra CP, Sakuma S, Gracia MP, Moralejo M, Molina-Cano JL, Komatsuda T, Igartua E. 2018. Resequencing the *Vrs1* gene in Spanish barley landraces revealed reversion of six-rowed to two-rowed spike. Molecular Breeding **38**, 51.

Chakraborty N, Kanyuka K, Jaiswal DK, Kumar A, Arora V, Malik A, Gupta N, Hooley R, Raghuram N. 2019. GCR1 and GPA1 coupling regulates nitrate, cell wall, immunity and light responses in *Arabidopsis*. Scientific Reports **9**, 5838.

Clifford H, Soderstrom T, Hilu K, Campbell C, Barkworth M. 1987. Grass systematics and evolution. Washington, DC: Random House (Smithsonian Institution Press).

Covington MF, Harmer SL. 2007. The circadian clock regulates auxin signaling and responses in *Arabidopsis*. PLoS Biology **5**, e222.

Dreni L, Kater MM. 2014. *MADS* reloaded: evolution of the *AGAMOUS* subfamily genes. New Phytologist **201**, 717–732.

Druka A, Franckowiak J, Lundqvist U, *et al*. 2011. Genetic dissection of barley morphology and development. Plant Physiology **155**, 617–627.

Ehlert A, Weltmeier F, Wang X, Mayer CS, Smeekens S, Vicente-Carbajosa J, Dröge-Laser W. 2006. Two-hybrid protein–protein interaction analysis in Arabidopsis protoplasts: establishment of a heterodimerization map of group C and group S bZIP transcription factors. The Plant Journal **46**, 890–900.

El-Brolosy MA, Kontarakis Z, Rossi A, Kuenne C, Günther S, Fukuda N, Kikhi K, Boezio GL, Takacs CM, Lai S-L. 2019. Genetic compensation triggered by mutant mRNA degradation. Nature **568**, 193–197.

Forster BP, Franckowiak JD, Lundqvist U, Lyon J, Pitkethly I, Thomas WT. 2007. The barley phytomer. Annals of Botany **100**, 725–733.

Gallagher JP, Man J, Chiaramida A, Rozza IK, Patterson EL, Powell MM, Schrager-Lavelle A, Multani DS, Meeley RB, Bartlett ME. 2023. *GRASSY TILLERS1* (*GT1*) and *SIX-ROWED SPIKE1* (*VRS1*) homologs share conserved roles in growth repression. Proceedings of the National Academy of Sciences, USA **120**, e2311961120.

Gaufichon L, Marmagne A, Belcram K, *et al*. 2017. *ASN1*-encoded asparagine synthetase in floral organs contributes to nitrogen filling in Arabidopsis seeds. The Plant Journal **91**, 371–393.

Gawroński P, Ariyadasa R, Himmelbach A, *et al.* 2014. A distorted circadian clock causes early flowering and temperature-dependent variation in spike development in the *Eps-3Am* mutant of einkorn wheat. Genetics **196**, 1253–1261.

Gottwald S, Bauer P, Komatsuda T, Lundqvist U, Stein N. 2009. TILLING in the two-rowed barley cultivar 'Barke' reveals preferred sites of functional diversity in the gene *HvHox1*. BMC Research Notes **2**, 258.

Hensel G, Kastner C, Oleszczuk S, Riechen J, Kumlehn J. 2009. *Agrobacterium*-mediated gene transfer to cereal crop plants: current protocols for barley, wheat, triticale, and maize. International Journal of Plant Genomics **2009**, 835608.

Hyun Y, Richter R, Vincent C, Martinez-Gallegos R, Porri A, Coupland G. 2016. Multi-layered regulation of SPL15 and cooperation with SOC1 integrate endogenous flowering pathways at the *Arabidopsis* shoot meristem. Developmental Cell **37**, 254–266.

Jayakodi M, Padmarasu S, Haberer G, *et al*. 2020. The barley pan-genome reveals the hidden legacy of mutation breeding. Nature **588**, 284–289.

Johannesson H, Wang Y, Engström P. 2001. DNA-binding and dimerization preferences of Arabidopsis homeodomain-leucine zipper transcription factors *in vitro*. Plant Molecular Biology **45**, 63–73.

Kellogg EA, Camara PEAS, Rudall PJ, Ladd P, Malcomber ST, Whipple CJ, Doust AN. 2013. Early inflorescence development in the grasses (Poaceae). Frontiers in Plant Science **4**, 250.

Kirby EM, Appleyard M. 1984. Cereal development guide. 2nd edn. Stoneleigh, UK: Arable Unit, National Agricultural Centre.

Komatsuda T, Nakamura I, Takaiwa F, Oka S. 1998. Development of STS markers closely linked to the *vrs1* locus in barley, *Hordeum vulgare*. Genome **41**, 680–685.

Komatsuda T, Pourkheirandish M, He C, *et al*. 2007. Six-rowed barley originated from a mutation in a homeodomain-leucine zipper I-class homeobox gene. Proceedings of the National Academy of Sciences, USA **104**, 1424–1429.

Koppolu R, Anwar N, Sakuma S, *et al*. 2013. *Six-rowed spike4* (*Vrs4*) controls spikelet determinacy and row-type in barley. Proceedings of the National Academy of Sciences, USA **110**, 13198–13203.

Koppolu R, Schnurbusch T. 2019. Developmental pathways for shaping spike inflorescence architecture in barley and wheat. Journal of Integrative Plant Biology **61**, 278–295.

Kuhlmann M, Horvay K, Strathmann A, Heinekamp T, Fischer U, Bottner S, Droge-Laser W. 2003. The α-helical D1 domain of the tobacco bZIP transcription factor BZI-1 interacts with the ankyrin-repeat protein ANK1 and is important for BZI-1 function, both in auxin signaling and pathogen response. The Journal of Biological Chemistry **278**, 8786–8794.

Langfelder P, Horvath S. 2008. WGCNA: an R package for weighted correlation network analysis. BMC Bioinformatics **9**, 559.

Li W, Wang H, Yu D. 2016. *Arabidopsis* WRKY transcription factors WRKY12 and WRKY13 oppositely regulate flowering under short-day conditions. Molecular Plant **9**, 1492–1503.

Li Y, Shen Y, Cai C, Zhong C, Zhu L, Yuan M, Ren H. 2010. The type II *Arabidopsis* formin14 interacts with microtubules and microfilaments to regulate cell division. The Plant Cell **22**, 2710–2726.

Livak KJ, Schmittgen TD. 2001. Analysis of relative gene expression data using real-time quantitative PCR and the $_2{}^{-\Delta\Delta C_T}$ method. Methods **25**, 402–408.

Ma Z, Zhu P, Shi H, Guo L, Zhang Q, Chen Y, Chen S, Zhang Z, Peng J, Chen J. 2019. PTC-bearing mRNA elicits a genetic compensation response via Upf3a and COMPASS components. Nature **568**, 259–263.

Nei M. 1987. Molecular evolutionary genetics. New York: Columbia University Press.

Peng J. 2019. Gene redundancy and gene compensation: an updated view. Journal of Genetics and Genomics = Yi Chuan Xue Bao **46**, 329–333.

Ramsay L, Comadran J, Druka A, *et al*. 2011. *INTERMEDIUM-C*, a modifier of lateral spikelet fertility in barley, is an ortholog of the maize domestication gene *TEOSINTE BRANCHED 1*. Nature Genetics **43**, 169–172.

Ranf S, Eschen-Lippold L, Pecher P, Lee J, Scheel D. 2011. Interplay between calcium signalling and early signalling elements during defence responses to microbe- or damage-associated molecular patterns. The Plant Journal **68**, 100–113.

Rozas J, Sanchez-DelBarrio JC, Messeguer X, Rozas R. 2003. DnaSP, DNA polymorphism analyses by the coalescent and other methods. Bioinformatics **19**, 2496–2497.

Ruijter J, Ramakers C, Hoogaars W, Karlen Y, Bakker O, Van den Hoff M, Moorman A. 2009. Amplification efficiency: linking baseline and bias in the analysis of quantitative PCR data. Nucleic Acids Research **37**, e45.

Saisho D, Pourkheirandish M, Kanamori H, Matsumoto T, Komatsuda T. 2009. Allelic variation of row type gene *Vrs1* in barley and implication of the functional divergence. Breeding Science **59**, 621–628.

Sakuma S, Golan G, Guo Z, *et al*. 2019. Unleashing floret fertility in wheat through the mutation of a homeobox gene. Proceedings of the National Academy of Sciences, USA **116**, 5182–5187.

Sakuma S, Lundqvist U, Kakei Y, *et al*. 2017. Extreme suppression of lateral floret development by a single amino acid change in the VRS1 transcription factor. Plant Physiology **175**, 1720–1731.

Sakuma S, Pourkheirandish M, Hensel G, *et al*. 2013. Divergence of expression pattern contributed to neofunctionalization of duplicated HD-Zip I transcription factor in barley. New Phytologist **197**, 939–948.

Sakuma S, Pourkheirandish M, Matsumoto T, Koba T, Komatsuda T. 2010. Duplication of a well-conserved homeodomain-leucine zipper transcription factor gene in barley generates a copy with more specific functions. Functional & Integrative Genomics **10**, 123–133.

Sakuma S, Salomon B, Komatsuda T. 2011. The domestication syndrome genes responsible for the major changes in plant form in the Triticeae crops. Plant and Cell Physiology **52**, 738–749.

Sambrook J, Russell DW. 2001. Molecular cloning. A laboratory manual. 3rd edn. Cold Spring Harbor: Cold Spring Harbor Laboratory Press.

Sessa G, Morelli G, Ruberti I. 1993. The Athb-1 and-2 HD-Zip domains homodimerize forming complexes of different DNA binding specificities. The EMBO Journal **12**, 3507–3517.

Shanmugaraj N, Rajaraman J, Kale S, *et al*. 2023. Multilayered regulation of developmentally programmed pre-anthesis tip degeneration of the barley inflorescence. The Plant Cell **35**, 3973–4001.

Shao J, Haider I, Xiong L, *et al*. 2018. Functional analysis of the HD-Zip transcription factor genes *Oshox12* and *Oshox14* in rice. PLoS One **13**, e0199248.

Thiel J, Koppolu R, Trautewig C, *et al*. 2021. Transcriptional landscapes of floral meristems in barley. Science Advances **7**, eabf0832.

Thirulogachandar V, Alqudah AM, Koppolu R, *et al*. 2017. Leaf primordium size specifies leaf width and vein number among row-type classes in barley. The Plant Journal **91**, 601–612.

Tian T, Liu Y, Yan H, You Q, Yi X, Du Z, Xu W, Su Z. 2017. agriGO v2. 0: a GO analysis toolkit for the agricultural community, 2017 update. Nucleic Acids Research 45, W122–W129.

Timmermans MC, Maliga P, Vieira J, Messing J. 1990. The pFF plasmids: cassettes utilising CaMV sequences for expression of foreign genes in plants. Journal of Biotechnology **14**, 333–344.

Tokunaga H, Kojima M, Kuroha T, Ishida T, Sugimoto K, Kiba T, Sakakibara H. 2012. Arabidopsis lonely guy (LOG) multiple mutants reveal a central role of the LOG-dependent pathway in cytokinin activation. The Plant Journal **69**, 355–365.

Ullrich SE. 2011. Barley. Production, improvement, and uses. Oxford: Wiley-Blackwell.

van Esse GW, Walla A, Finke A, Koornneef M, Pecinka A, Von Korff M. 2017. Six-rowed spike 3 (VRS3) is a histone demethylase that controls lateral spikelet development in barley. Plant Physiology **174**, 2397–2408.

Waddington SR, Cartwright PM, Wall PC. 1983. A quantitative scale of spike initial and pistil development in barley and wheat. Annals of Botany **51**, 119–130.

Wang Y, Yu H, Tian C, Sajjad M, Gao C, Tong Y, Wang X, Jiao Y. 2017. Transcriptome association identifies regulators of wheat spike architecture. Plant Physiology **175**, 746–757.

Wu T-Y, Krishnamoorthi S, Goh H, Leong R, Sanson AC, Urano D. 2020. Crosstalk between heterotrimeric G protein-coupled signaling pathways and WRKY transcription factors modulating plant responses to suboptimal micronutrient conditions. Journal of Experimental Botany **71**, 3227–3239.

Wu Z, Li T, Zhang Y, Zhang D, Teng N. 2024. HD-Zip I protein LlHOX6 antagonizes homeobox protein LlHB16 to attenuate basal thermotolerance in lily. Plant Physiology, doi: 10.1093/plphys/kiad582.

Yoo SD, Cho YH, Sheen J. 2007. *Arabidopsis* mesophyll protoplasts: a versatile cell system for transient gene expression analysis. Nature Protocols **2**, 1565–1572.

Youssef HM, Eggert K, Koppolu R, *et al*. 2017. VRS2 regulates hormone-mediated inflorescence patterning in barley. Nature Genetics **49**, 157–161.

Zhao M, Yang S, Chen C-Y, Li C, Shan W, Lu W, Cui Y, Liu X, Wu K. 2015. *Arabidopsis* BREVIPEDICELLUS interacts with the SWI2/SNF2 chromatin remodeling ATPase BRAHMA to regulate *KNAT2* and *KNAT6* expression in control of inflorescence architecture. PLoS Genetics **11**, e1005125.

Zwirek M, Waugh R, McKim SM. 2019. Interaction between row-type genes in barley controls meristem determinacy and reveals novel routes to improved grain. New Phytologist **221**, 1950–1965.